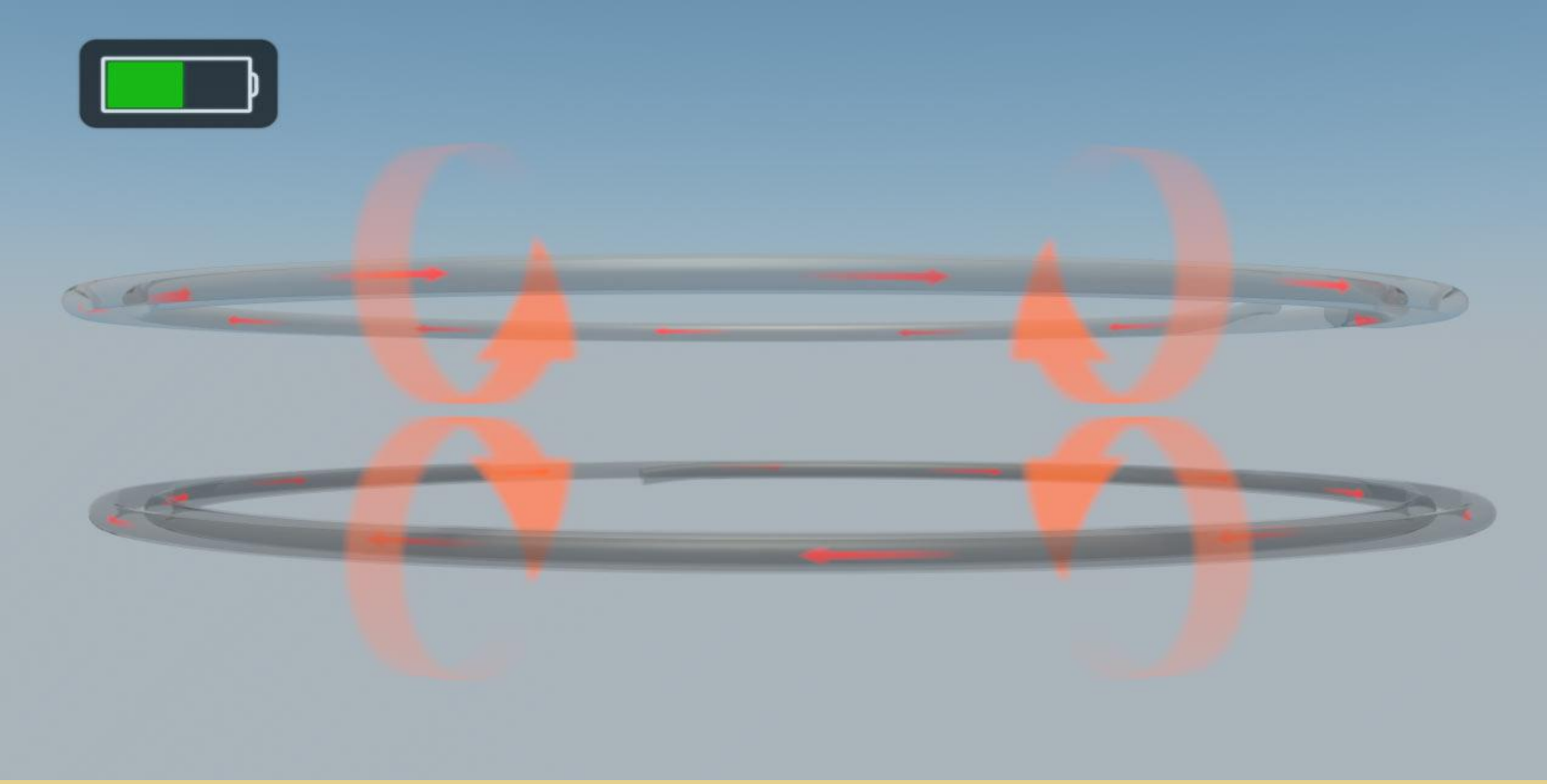

Abdallah Toni Satel

Wireless Charger for Low Power Devices

Master's Thesis in Electrical and Computer Engineering
Specialization in Telecommunications

July/2016

· U C ·

UNIVERSIDADE DE COIMBRA

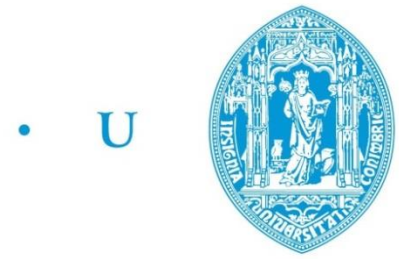

UNIVERSIDADE DE COIMBRA
FCTUC
FACULDADE DE CIÊNCIAS E TECNOLOGIA

Master's Thesis in Electrical and Computer Engineering

Specialization in Telecommunications

Wireless Charger for Low Power Devices

By Student

Abdallah Toni Satel

Jury

President – Dr. Aníbal Traça de Carvalho Almeida
Advisor – Dr. André Manuel dos Santos Mendes
Vowel – Dr. Jaime Baptista dos Santos

July/2016

Acknowledgments

First of all, I would like to express my sincere gratitude to my professor and advisor Dr. André Manuel dos Santos Mendes, who introduced me to the realm of wireless power transfer. Without his guidance, encouragement, and support this project would not have been completed. He has always inspired me to work hard and has instilled the belief in me that with hard work, any goal can be achieved. It has truly been a privilege to work under his guidance.

I would also sincerely like to specially thank the former president of Portugal Mr. Jorge Sampaio the founder of global platform for Syrian students and Dr. Helena Barroco the diplomatic adviser to the president for giving me the opportunity to continue and complete my Master in Portugal.

I would then like to thank the University of Coimbra and its president Dr. João Gabriel Silva for offering me the scholarship in it and also for Dr. Teresa Baptista for the all help she provides in Coimbra.

I would also like to thank my colleagues at the laboratory for all their help and advice in both academic and non-academic.

Last but not the least, my family who are my inner strength and whom I represent in all walks of my life.

Abstract

Wireless power transfer technology has been widely used in many areas. This thesis implements a wireless charging system for consumer electronics for mobile applications such as laptops and tablets. The working on a wireless power transfer system is comparable to that of an air core transformer with the leakage compensated by means of capacitances. Compensation has been applied to both the primary and secondary of the transformer. This would help boost power transfer. Theoretically described the basic series-series compensation topology used. The resonant wireless power transfer is demonstrated in this thesis. The efficiency of such a system is analyzed and the results are promising, however, there are significant opportunities for improvement.

Table of contents

List of Figures

List of Tables

List of Abbreviations

ω Resonance frequency

μ_0 Permeability of the air

AC Alternating current

C capacitor

C1 primary capacitor

C2 secondary capacitor

DC Direct current

EM electromagnetic

F frequency

FHA First Harmonics Approximation

Fr resonance frequency

Fs switching frequency

H Height

H-bridge full bridge inverters

I Current

i1 (t) instantaneous current value at AC circuit at primary side

I1 RMS current value at AC circuit in primary side

i2 (t) instantaneous current value at AC circuit at secondary side

I2 RMS current value at AC circuit in secondary side

idc (t) instantaneous current value at DC circuit at primary side

Idc RMS current value at DC circuit in primary side

iload (t) instantaneous current value at DC circuit at secondary side

ILoad RMS current value at DC circuit in secondary side

K Coupling coefficient

L1 primary inductance

L2 secondary inductance

M mutual inductance

N1 number of turns in primary coil

N2 number of turns in secondary coil

p1 (t) instantaneous power value at AC circuit at primary side

P1 RMS power value at AC at primary side

p2 (t) instantaneous power value at AC circuit at secondary side

P2 RMS power value at AC at secondary side

p3 (t) instantaneous power value at DC circuit at secondary side

PC Personal computer

pdc (t) instantaneous power value at DC circuit at primary side

Pdc RMS power value at DC at primary side

Pload RMS power value at DC at secondary side

PP Parallel-Parallel

PS Parallel-Series

Q quality factor

R1 equivalent radius of the primary windings

R2 equivalent radius of the secondary windings

Res1 primary resistor

Res2 secondary resistor

RL equivalent load resistance

RLoad terminal load resistance (battery)

RMS Root mean square

S1 section of the windings in primary coil

S2 section of the windings in secondary coil

SP Series-Parallel

SS Series-Series

v1 (t) instantaneous voltage value at AC circuit in primary side

V1 RMS voltage value at AC circuit in primary side

v2 (t) instantaneous voltage value at AC circuit in secondary side

V2 RMS voltage value at AC circuit in secondary side

vdc (t) instantaneous voltage value at DC circuit in primary side

Vdc RMS voltage value at DC circuit in primary side

vload (t) instantaneous voltage value at DC circuit in secondary side

VLoad RMS voltage value at DC circuit in secondary side

WPT Wireless Power Transfer

Z2 total impedance of the secondary side

ZCS zero-current switching

ZPA zero phase angle

Ztotal Total system impedance

ZVS zero voltage switching

η efficiency

CHAPTER 1

Motivations and Introduction About Wireless Power Transfer

1.1 History of Wireless Power Transfer

The history of wireless power transmission dates back to the late 19th century with the prediction that power could be transmitted from one point to another in free space by Maxwell in his Treatise on Electricity and Magnetism. Heinrich Rudolf Hertz performed experimental validation of Maxwell's equation which was a monumental step in the direction. However, Nikola Tesla's experiments are often considered as being some of the most serious demonstrations of the capability of transferring power wirelessly even with his failed attempts to send power to space[1].

In the last few years, the electric car industry has shown an increased interest in the possibility to charge vehicles wirelessly. Wireless charging stations at parking lots could ensure that your car is charged when it is time for departure. On the regular road network, wireless charging stations could be placed at intersections or along longer stretches of road, extending the operational distance of electric cars. Other applications can benefit from advances in wireless energy transfer, e.g. electric trucks in a warehouse can operate continuously if the floor is equipped with wireless charging tracks. However, simultaneous high efficiency and high power transfer in wireless energy transfer system has proven difficult to achieve over moderate distances in air.

Using strongly magnetic resonance, the WiTricity research group led by MIT wirelessly powered a 60 W bulb with 40 % power efficiency at a distance of 2 m. Intel reproduced the original 1894 implementation of electrodynamic induction by wirelessly powering a nearby light bulb with 75% efficiency. Sony showed a wireless electrodynamic-induction powered TV set, 60 V over 50 cm. Haier showed a wireless LCD TV at CES 2010 using researched Wireless Home Digital Interface. In this period, our research team focused on the wireless power transfers for biomedical applications [4].

1.2 Classification of Wireless Power Transfer Systems

Wireless power transfer systems can be classified into different types depending on various factors. On the basis of the distance from the radiating source, the characteristics of the EM fields change and so are the methods for achieving wireless power transfer. They can be categorized as:

1. Near field
2. Mid field
3. Far field

In case of near field radiation, the boundary between the regions is restricted to one wavelength. In the transition zone, the boundary between the regions is between one to two wavelengths of electromagnetic radiation. In case of far field, the distance between the radiating source and the receiver is more than twice the wavelength of the radiation [2].

Based on the mode of coupling between the transmitter and the receiver, wireless power transfer techniques [11] can be classified into the following:

1. Electromagnetic induction (Resonant Wireless Power Transfer)
2. Electrostatic induction (Resonant Capacitive Power Transfer)
3. Far field transfer techniques (Laser and Microwave Power Transfer)

Table 1.1 Summary of advantages and disadvantages of different WPT technologies

WPT Technology Category	Advantages	Disadvantages
Inductive coupling	Sample, safe and high transfer efficiency in short distance	Short transmission distance, needs accurate alignment
Magnetic Resonant Coupling	Long transmission distance, no radiation	Difficult to adjust resonant frequency for multiple devices
Electromagnetic Radiation	Very high transmission efficiency over long distance	Radiation, needs line of sight

1.3 Types of Wireless Power Transfer

The ability of the technology to transfer power safely, efficiently, and over distance will improve products by making them more convenient, reliable, and environmentally friendly. Wireless power transfer technology can be used to provide two different types [3].

- **Automatic Wireless Charging**

A device with rechargeable batteries charges itself, while still in use or at rest, without requiring a power cord or battery replacement. This mode is used to charge mobile devices when in range of its power source, without having to physically connect the device.

- **Direct Wireless Power**

All the power that a device needs is provided wirelessly, no batteries are required. This mode powers devices that are always within range of its power source.

1.4 Applications of Wireless Power Transfer Systems

Wireless power transfer technology can be applied across a wide variety of applications and environments [3] such as

- **Consumer electronics products:**

  Automatic wireless charging of mobile electronics such as phones, laptops, game controllers, wearables - in homes, cars, offices, public hotspots, even while the devices are in use in some cases. Direct wireless powering of stationary devices, like flat screen TVs, desktop PC peripherals such as wireless mice, keyboards, printers, speakers, displays eliminating disposable batteries and cabling.

- **Automotive applications:**

  Automatic wireless charging for future hybrid and all electric passenger and commercial vehicles, at home, in parking garages, in vehicle wireless charging for mobile devices while driving by reducing the need for power cords.

- **Industrial applications:**

  Direct wireless power and communication interconnections across rotating and moving joints for robots as packaging machinery, assembly machinery by eliminating the need for expensive power wiring or battery replacement and disposal. Automatic wireless charging for mobile robots, autonomous vehicles, cordless tools and instruments.

- **Medical applications:**

  Direct wireless power interconnections and automatic wireless charging for implantable medical devices. Implantable therapies that require substantial power to operate up to 10s of watts become practical as they no longer require drive lines that penetrate the skin.

- **Military equipment:**

  Automatic wireless charging for high tech military systems, such as battery powered mobile devices, covert sensors, unmanned mobile robots and aircraft, wireless power transfer to power helmet mounted devices and to defog optics. Vehicle seat back to solder vest wireless power transfer to charge central batteries while seated in transport vehicles

1.5 Market of Wireless Power Transfer Systems

Wireless Power is a fast growing market more than 140 million wireless charging receivers were sold last year, and more than 50 million wireless chargers. The market research company IHS predicts that the market for wireless charging will continue to double in size in the coming years. In 2018 a market worth $8.5 billion is forecast with strongest adoption in mobile phones and tablet PCs. Wearable technology is also predicted to provide strong demand for wireless power from 2014. Wireless power can potentially be used in any application where charging or a direct power source is required, therefore a large number of other opportunities exist [3].

1.6 Project Outlines

This thesis consists of five chapters, after this chapter we will see:

Chapter 2 Introduction about the fundamentals of wireless power transfer system: talking about the theoretical study of the compensation topology and determines the important elements of such a system to help the design of a wireless power transfer system to be good.

Chapter 3 Defines the parameters of the desired design by using Matlab codes and Matlab model simulation and comparison for the results.

Chapter 4 Implement the study of the experimental system, and compare the result with its own simulated and calculated results.

Chapter 5 at the end, we will see the conclusion of the project and the future work.

CHAPTER 2

Theory Fundamentals of Wireless Power Transfer Systems

2.1 Basic of Wireless Power Transfer

In WPT system the power is transferred inductively from one coil to another, which is due to the mutual inductance between these two coils. The principle is generally the same as for a transformer. The main difference is that in a transformer the coupling between the two sides is high, whereas in a WPT system the coupling is low due to the large air gap between the coils or magnetic material. Many WPT systems do not use ferrite or other magnetic materials and the flux therefore travels through air. These systems has reduced coupling, but on the other hand they have no core losses. The low coupling causes relatively big leakage inductance on both sides of the transformer and a reduced magnetization flux. A bigger magnetization current is therefore needed to increase the flux.

2.1.1 Typical WPT System

A typical WPT system that draws from the AC mains to charge a battery is shown in Fig 2.1 the inverter usually provides a high-frequency square wave voltage to the primary resonant tank (primary coil and compensation) the resonant tank at the secondary circuit will output square-wave voltage when there is rectifier with a battery load. First harmonics approximation (FHA) can be used to convert the square-wave voltage source into a sinusoidal voltage source, and the rectified battery load into a resistive load [6]. Modelling a linear source and a load in this way, we can analyze the WPT system using any of the lumped circuit models as shown in Fig 2.2

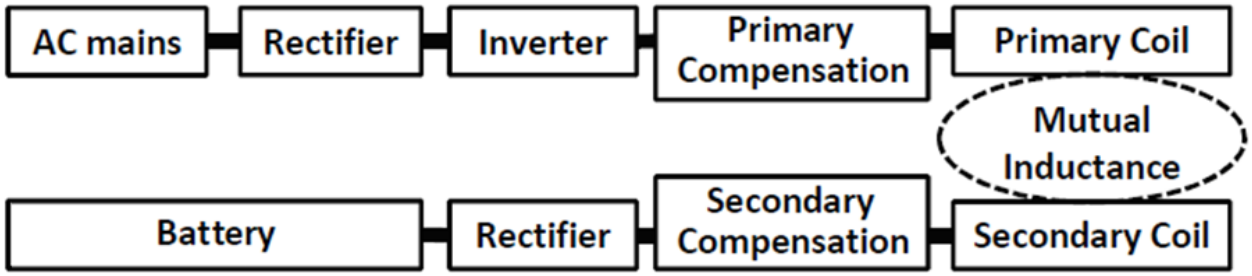

Fig 2.1 Typical WPT system charging battery

2.2 Compensation Topologies

There is no fixed rule for choosing the topology. There are four basic compensation topologies for wireless power transfer as shown in Fig 2.2 they are Series-Series (SS), Series-Parallel (SP), Parallel-Series (PS), and Parallel-Parallel (PP).

By comparing Fig 2.2 with Fig 2.1 we can see that C1 is equivalent to the primary compensation, L1 is equivalent to the primary coil, M is equivalent to the mutual inductance between the two coils, L2 is the secondary coil and C2 is the secondary compensation, any of the four compensation topologies can be used depending on the system design.

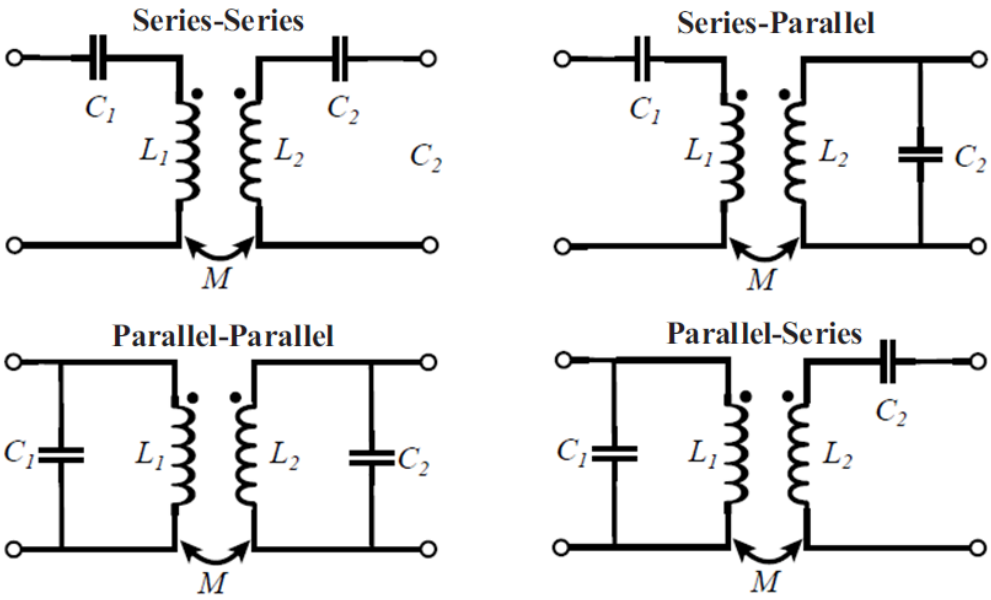

Fig 2.2 Basic compensation topologies

2.2.1 Choice between SS and SP topology

A very important feature that the primary series compensation topologies possess is that the choice of their compensation capacitances is independent of the load which is a desirable property particularly when the loading profile is variable. The choice between the two primary series compensation strategies would in turn depend on various factors such as efficiency and its tolerance to variable frequencies, the desired power levels of operation, power factor and its tolerance to variable frequencies and cost. It can be generally observed that for higher power levels, Series-parallel compensation can transfer high powers at low voltage and high current. In case of Series-series compensation, due to its comparatively large impedance at resonant frequency, the currents drawn at low voltages are not very high and hence high power transfer can take place only at high voltages. In case of variable frequency operations, it is desirable to go for Series-series topology as it has higher tolerance for power factor when frequency changes.

It can be observed that the maximum efficiency for Series-series topology is much higher than that of Series-parallel topology. Hence, for fixed frequency systems, it would be better to select for Series-series topology. However, frequency tolerance for efficiency is better in case of Series-series topology over Series-parallel topology particularly at super-resonant frequencies. For sub-resonant frequencies, the efficiencies in case of Series-parallel topology are higher than that of Series-series topology [7].

However, selection of both the primary and secondary compensation capacitances is based on two different criterions:

1. The secondary capacitance is chosen as the first step. This is done in such a manner so as to compensate the secondary leakage inductance and the mutual inductance. This type of compensation would lead to an improvement in the power transferred to the load.
2. The primary capacitance is then chosen such that it considers the inductance of the entire circuit. In literature, primary capacitances chosen to compensate just the self-inductance of the primary and the inductance of the entire circuit are present. However, it is a better choice to perform compensation for the entire circuit so that the input power factor becomes unity.

2.2.2 Series-Series topology

For this project design a Series-series compensation topology where chosen because, the primary components with the capacitor C1 behaves like a current source and will produce a constant output current [12], that would result in an induced voltage in the secondary coil with a constant amplitude. The second series capacitor C2 was added to ensure fixed resonant frequency independent of coupling and load and acts as a voltage source that supplied a stable voltage.

Therefore it is wise to go for Series-Series topology for battery charging for both constant voltage charging as well as constant current charging [7].

Fig 2.3 demonstrates the equivalent circuit of Series-Series topology. The parameters of the equivalent circuit are explained in Section 2.5

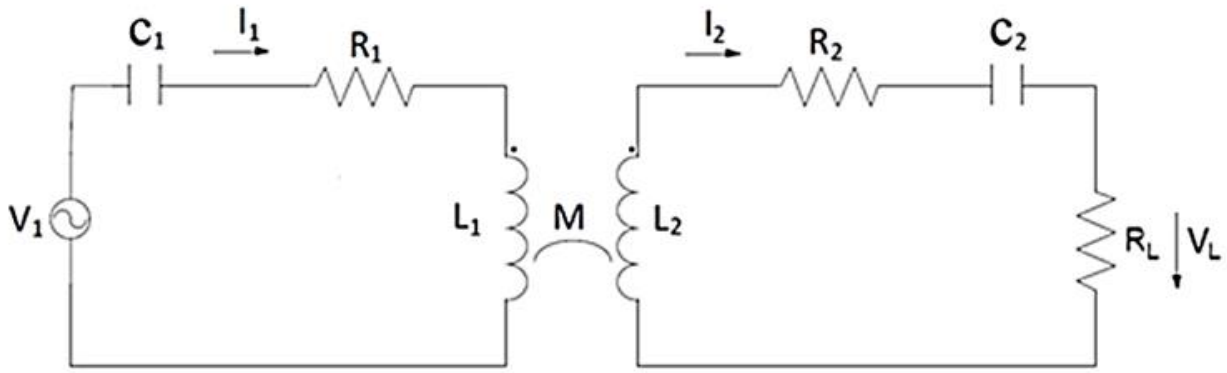

Fig 2.3 Series-series compensation equivalent circuit

2.2.3 Modes of Operation

In order to improve the power transfer efficiency, two main strategies can be used:

1. Soft switching technique: zero voltage switching (ZVS) or zero-current switching (ZCS) in order to reduce the switching loss of the resonant inverter.

2. Compensation network or impedance matching: the poor coupling of the windings is balance by adding parallel or series capacitors at the primary and the secondary. The compensated circuit is designed so the zero phase angle (ZPA) on the primary side is obtained at the resonance frequency. That is, in order to achieve the maximum output power with the minimum input VA rating (that reduces the cost). ZPA have been used commonly.

Fig 2.4 shows a plot of the resonant tank gain K with the normalized switching frequency for different values of Quality factor Q and any single value of m, m=6 was used as an example.

The working regions ZCS region is marked in red color and the region of ZVS is marked in white color.

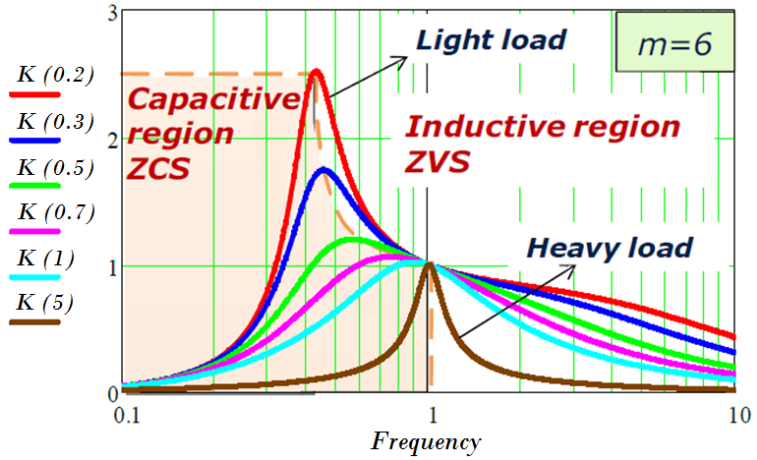

Fig 2.4 ZCS and ZVS working regions

The converter can operate in three modes [5] depending on input voltage and load current conditions, as listed below and shown in Fig 2.5

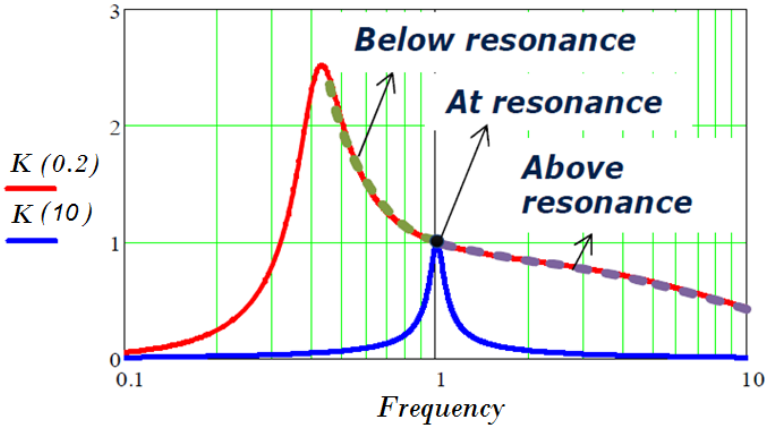

Fig 2.5 Modes of operation

1. At resonant frequency operation fs=fr.
2. Above resonant frequency operation fs>fr.
3. Below Resonant frequency operation fs<fr.

2.3 Coil Considerations

2.3.1 Coil Design

In the WPT system there are several parameters that can be used to find the best shape and size of the coils.

These parameters are:

- Mutual inductance M
- Real power transferred P_2
- Power transfer efficiency η
- Coupling coefficient k

We will talk about them later in this chapter.

2.3.2 Coil Shape

Two designs have mostly been used for coils in the WPT systems, circular and rectangular. In this project design rectangular shape coils were chosen because rectangular coils offer good coupling and high misalignment consideration [9]. The primary rectangular coil will be placed under the table and the secondary pickup coil will be placed under the laptop over the table. This design will give the user the flexibility and the freedom to change the position of the laptop to left or right of the table while charging. Fig 2.6 show the diagram of the model implemented.

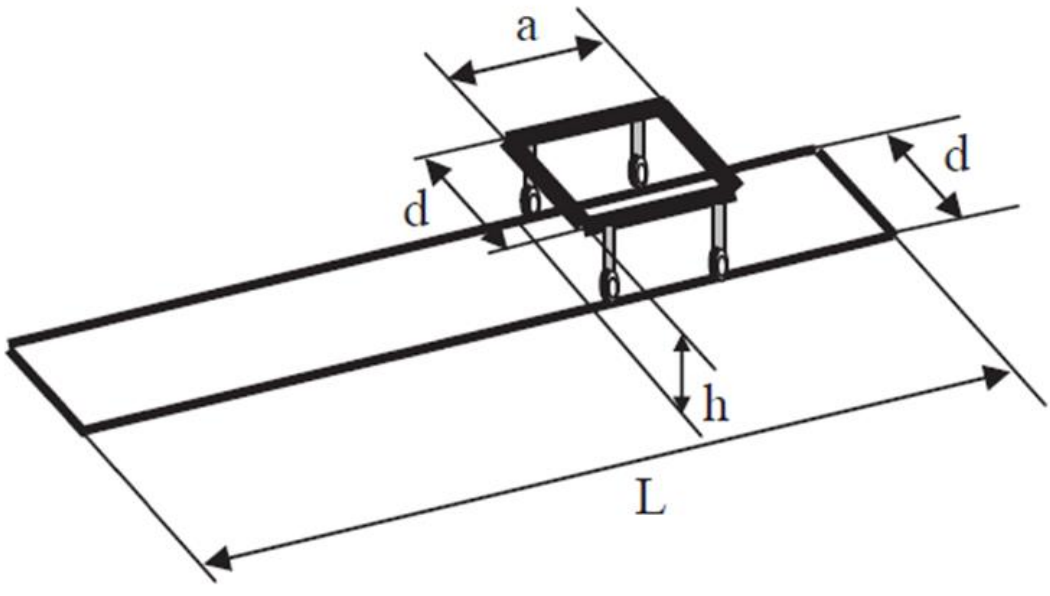

Fig 2.6 Diagram showing the notation used for the coils

2.3.3 Circuit Parameters Calculation

To obtain the theoretical inductance values of L_1, L_2 and M the following expressions must be used [8].

L_1 is given by

$$L_1 = \frac{\mu_0}{\pi} {N_1}^2 \left(d.ln \frac{2.L.d}{R_1(d+\sqrt{L^2+d^2})} \right) \quad (2-1)$$

$$+ \frac{\mu_0}{\pi} {N_1}^2 \left(L.ln \frac{2.L.d}{R_1(L+\sqrt{L^2+d^2})} - 2(d+L-\sqrt{d^2+L^2}) \right) + \frac{\mu^0}{4\pi} {N_1}^2 (\mathrm{L}+\mathrm{d})$$

And L_2 is given by

$$L_2 = \frac{\mu_0}{\pi} {N_2}^2 \left(d.ln \frac{2.a.d}{R_2(d+\sqrt{a^2+d^2})} \right) \quad (2-2)$$

$$+ \frac{\mu_0}{\pi} {N_2}^2 \left(a.ln \frac{2.a.d}{R_2(a+\sqrt{a^2+d^2})} - 2(d+a-\sqrt{d^2+a^2}) \right) + \frac{\mu_0}{4\pi} {N_2}^2 (\mathrm{a}+\mathrm{d})$$

Where R_1 and R_2 are the equivalent radius of the windings

$$R_1 = \frac{\sqrt{N_1 S_1}}{\pi} \quad (2-3)$$

$$R_2 = \frac{\sqrt{N_2 S_2}}{\pi} \quad (2-4)$$

S_1 and S_2 are the radius section of the windings.

The mutual inductance coefficient M when the two coils have the same dimensions is given by

$$M = \frac{\mu_0}{\pi} N_1 N_2 \left(d.ln \frac{d+(\sqrt{h^2+d^2})(\sqrt{h^2+a^2})}{d+h\sqrt{h^2+d^2+a^2}} \right) \quad (2-5)$$

$$+ \frac{\mu_0}{\pi} N_1 N_2 \left(a.ln \frac{a+(\sqrt{h^2+d^2})(\sqrt{h^2+a^2})}{a+h\sqrt{h^2+d^2+a^2}} \right)$$

$$+ \frac{\mu_0}{\pi} N_1 N_2 \left(2(h-\sqrt{h^2+d^2}-\sqrt{h^2+a^2}+\sqrt{h^2+d^2+a^2}) \right)$$

Considering a case where the primary track is longer than the secondary pick up **L** >> **a** which is used in this thesis, [8] the mutual inductance can be approximated by

$$M = \frac{\mu_0}{\pi} N_1 N_2 \, al\, n \left(\frac{\sqrt{h^2+d^2}}{h} \right) \quad (2-6)$$

Where μ_0 is the permeability of the air and have a constant value equal to $4\,.\pi.10^{-7}\ H.m^{-1}$

The resistive values of the windings can be calculated by

$$Res_1 = \frac{1}{57} N_1 \frac{2(L+d)}{S_1} \qquad (2-7)$$

$$Res_2 = \frac{1}{57} N_2 \frac{2(a+d)}{S_2} \qquad (2-8)$$

2.3.4 Operational Frequency

The frequency can be calculated by

$$f = \frac{1}{2\pi\sqrt{LC}} \qquad (2-9)$$

The Capacitors C_1 and C_2 must be selected at the secondary resonant frequency in order to achieve maximum power transfer capability [8].

The resonant compensation capacitances can be calculated by

$$C_1 = \frac{1}{\omega^2 L_1} \qquad (2-10)$$

$$C_2 = \frac{1}{\omega^2 L_2} \qquad (2-11)$$

2.4 Power transfer capability

2.4.1 Coupling coefficient

The wireless power transfer capability of a WPT system depends directly on the coupling coefficient k [8], which is given by

$$k = \frac{M}{\sqrt{L_1 L_2}} \qquad (2-12)$$

2.4.2 Impact of coupling coefficient and frequency on the efficiency of WPT

The coupling coefficient between the primary and secondary can be calculated from (2-12) if no coupling exists between the primary and secondary, then M=0 and thus k=0. The general transformers with cores and no air gap have the highest coupling coefficient. The coupled coils that have $k > 0.5$ are termed as tightly coupled and those having $k < 0.5$ are called loosely coupled. The value of M and thereby k depends on the physical dimensions and the number of turns of each coil, their relative position to one another and the magnetic properties of the core on which they are wound [9]. To improve the coupling between the coils it is recommended to increasing the number of turns on the primary and secondary coils, using Litz wire, and also by using ferrite bars materials to short the magnetic path [13]. The better the coupling between the two coils, the lower of the design frequency.

2.4.3 Inductor quality factor

The quality factor quantifies how much the coil is purely inductive. It signifies its ability to produce a large magnetic field. Normally, the WPT system is designed to operate at a fixed frequency, however, sometimes, due to a change in parameters, i.e. capacitance or load, the air gap causes the change in system frequency, so the transfer efficiency drops. Therefore the system does not operate at a zero phase angle frequency [9] [10]. The native quality factor of primary and secondary coil can be calculated as quality factor is a measure on how ideal an inductor is and is derived by

$$Q_1 = \frac{\omega\, L_1}{Res_1}\,, \qquad Q_2 = \frac{\omega\, L_2}{Res_2} \tag{2-13}$$

Where:

$\omega = 2\pi f$

f is the frequency.

L_1, L_2 is the inductance.

Res_1, Res_2 are the wire resistance.

An ideal inductor has no resistive loss resulting in an infinite quality factor, but all real inductors have at least some wire resistance. For low frequencies designs the resistive value of solid copper wire is small but for high frequencies the resistive value of solid copper wire increase by increasing the frequency. To avoid this effect which is called the skin effect, Litz-wire should be used which has low resistive values at high frequencies.

2.5 Prototype Model Design

2.5.1 WPT full circuit model

The full wireless power transfer system model divided into five sections as shown in Fig 2.7

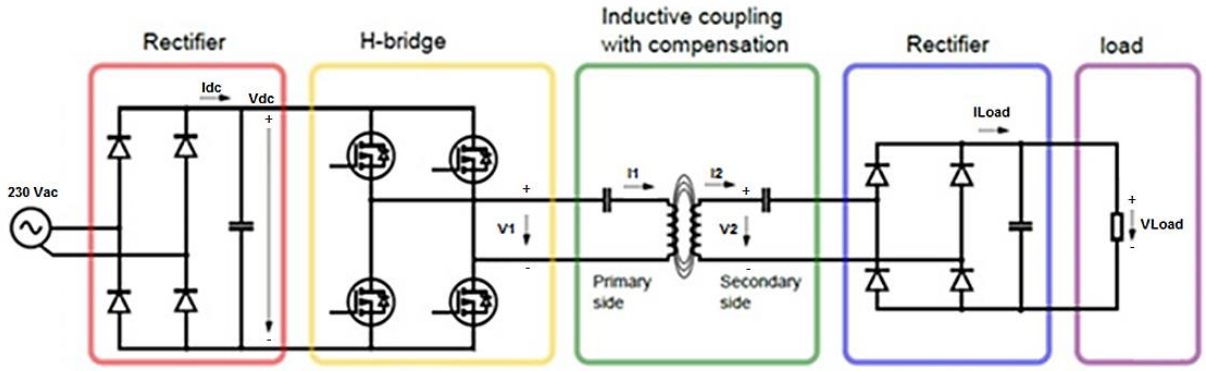

Fig 2.7 Wireless power transfer (WPT) system divided into five sections

By comparing each section of Fig 2.7 with the typical WPT system in Fig 2.1 we can see the red section is equivalent to the AC main with the rectifier at the primary side and the yellow section is equivalent to the inverter. The green section is equivalent to the primary compensation circuit with the primary coil, as well the secondary coil with the secondary compensation circuit. The blue section is equivalent to the rectifier on the secondary side of Fig 2.1 and the last purple section is equivalent to the battery load.

In Fig 2.7 the DC output voltage from the two phase rectifier will be converted from 230V AC transformer. In this project the main focus will only be on the power transfer between the two coils, therefore the grid and the rectifiers will be replaced with a DC power supply which can deliver the desired voltage for the design. The H-bridge inverters have a fundamental frequency that matches the resonance frequency of the series compensation circuit. Power IGBTs inverters where used in this project.

Previously the convenience of having a compensation circuit was explained and the chosen topology of compensation depends on the application of the WPT system was explained in Section 2.2

Misalignment and distance (height) between transfer and pickup coil and is also an issue for a WPT system. This has influence on the mutual inductance and coupling coefficient. Different coil shape and sizes has a different advantage which was also defined in Section 2.3

For charging the batteries of a laptop the transfer coil is placed under the table and the pickup underneath the laptop, the height would normally be between 2-4, cm but this is dependent from table to table. In this report the height between the primary and secondary coils is set to be 3 cm.

2.5.2 Equivalent circuit analysis of WPT system

To simplify the understanding of how the full WPT system in Fig 2.7 and how the WPT system was transformed to its equivalent circuit as in Fig 2.12, the following steps below explain the transformation of each section of the circuit.

In Fig 2.8 the first two sections of Fig 2.7 AC mains, rectifier and H-bridge inverters are equivalent to the AC voltage source V1 of Fig 2.12

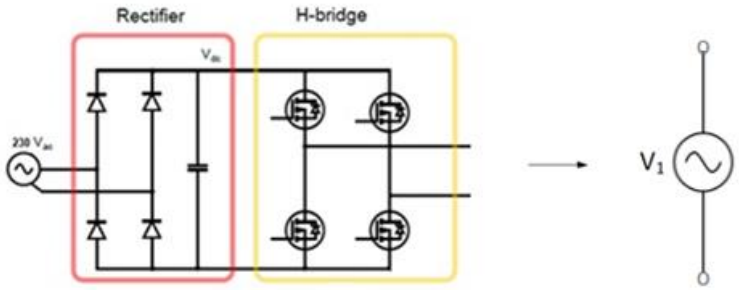

Fig 2.8 Equivalent circuit of voltage source V1

As we can see from Fig 2.7, the mutual inductance M of the inductors L1 and L2 with series-series compensation C1 and C2 as shown in Fig 2.9 are equivalent in the circuit to

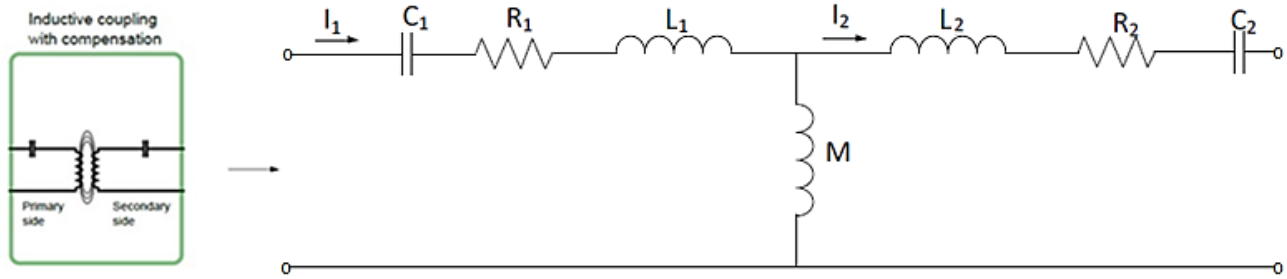

Fig 2.9 Equivalent circuit of the mutual inductance M

The rectifiers and the equivalent load resistance from Fig 2.7 are equivalent to the load resistance RL in the secondary side of the equivalent circuit as shown in Fig 2.10

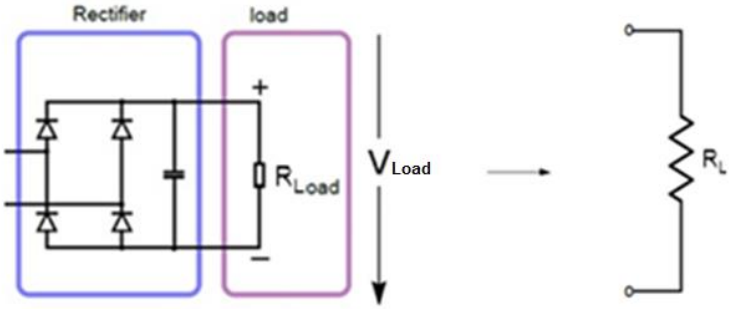

Fig 2.10 Equivalent circuit of the circuit resistance as defined as RL

The terminal load resistance RL is equivalent to a battery of a laptop or mobile as in Fig 2.11

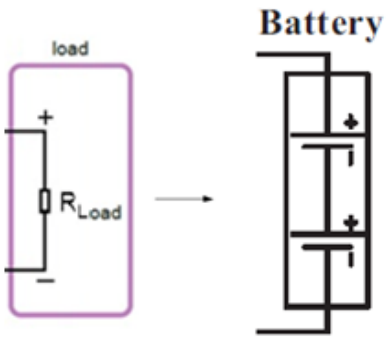

Fig 2.11 Equivalent circuit of the load resistance RL

2.5.3 Equivalent circuit equations of WPT system

Fig 2.3 and Fig 2.12 illustrates the full series-series WPT equivalent circuit model, where Z_2 is the total impedance of the secondary side Z_2 as seen by the primary coil.

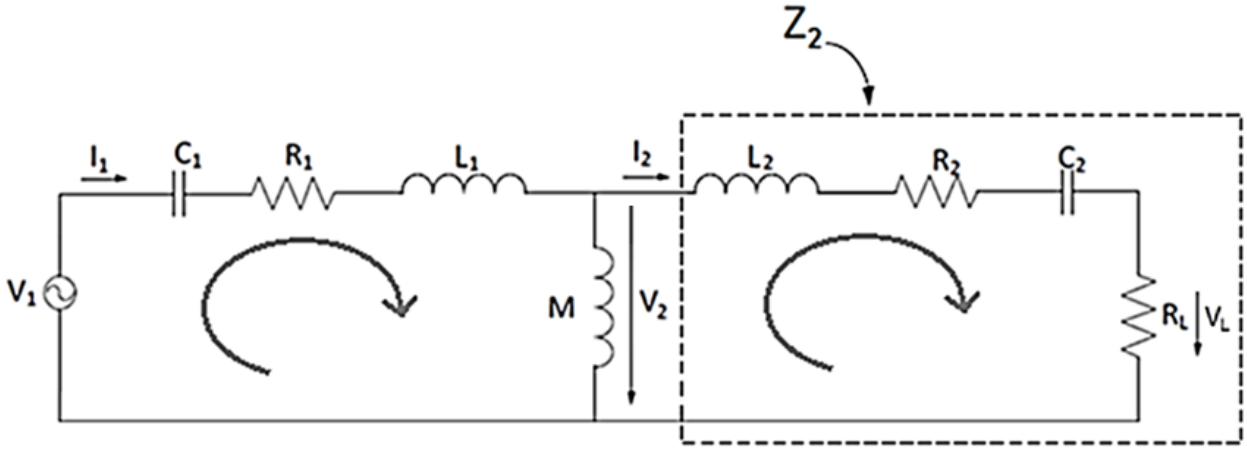

Fig 2.12 Equivalent circuit of series-series WPT system

Considering the WPT system with compensation as in Fig 2.12 the following equations can be established according to Kirchhoff's 2nd law:

$$V_1 = I_1\left(\frac{1}{j\omega c_1} + R_1 + jwL_1\right) + j\omega M(I_1 - I_2) \qquad (2-14)$$

$$0 = I_2\left(jwL_2 + R_2 + \frac{1}{j\omega c_2} + R_L\right) + j\omega M(I_2 - I_1) \qquad (2-15)$$

The equivalent load resistance in the circuit is calculated by

$$R_L = \frac{8n^2}{\pi^2} R_{Load} \qquad (2-16)$$

Where n is the ratio between the number of turns in the primary coil and the secondary coil

$$n = \frac{N_1}{N_2} \qquad (2-17)$$

RLoad is the terminal load at DC circuit, calculated by

$$R_{Load} = \frac{V_{Load}}{I_{Load}} \qquad (2-18)$$

Fig 2.13 illustrate the equivalent circuit when all the quantities are referred to the primary side

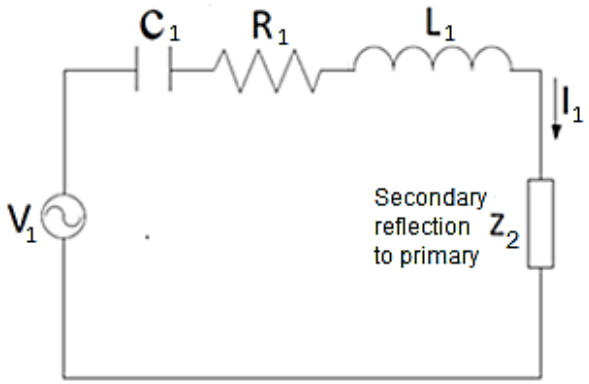

Fig 2.13 WPT equivalent RLC circuit as seen by the primary side

The current through the primary coil I_1 is determined by the input voltage V_1 and the total impedance of the secondary side Z_2 as seen by the primary coil. When the primary side is series compensated the current through the primary coil is

$$I_1 = \frac{V_1}{Z_{Total}} \qquad (2-19)$$

Where Ztotal is the impedance of the primary and secondary and it is given by

$$Z_{Total} = R_1 + j\omega L_1 + \frac{1}{j\omega c_1} + \frac{\omega^2 M^2}{Z_2} \qquad (2-20)$$

And Z_2 is the total impedance of the secondary reflection to the primary side [9] it is given by

$$Z_2 = R_2 + \frac{1}{j\omega c_2} + j\omega L_2 + R_L \qquad (2-21)$$

By applying $(2-21)$ in $(2-20)$, I_1 can be rewritten as

$$I_1 = \frac{V_1}{R_1 + j\omega L_1 + \frac{1}{j\omega c_1} + \frac{\omega^2 M^2}{R_2 + \frac{1}{j\omega c_2} + j\omega L_2 + R_L}} \qquad (2-22)$$

When the circuit is operating at f_r resonant frequency LC components cancel out their reactance, I_1 is given by

$$I_1 = \frac{V_1}{R_1 + \left(\frac{\omega^2 M^2}{R_2 + R_L}\right)} \qquad (2-23)$$

The current through the second coil is given by the induced voltage divided by the total impedance of the secondary circuit side

$$I_2 = \frac{j\omega M\, I_1}{Z_2} \qquad (2-24)$$

And can be rewritten as

$$I_2 = \frac{j\omega M\, I_1}{R_2 + \frac{1}{j\omega c_2} + j\omega L_2 + R_L} \qquad (2-25)$$

The voltage induced in the secondary coil V_2 is proportional to the current through the primary coil I_1

$$V_2 = j\omega M\,(I_1 - I_2) \qquad (2-26)$$

2.5.4 Efficiency

The parameters used in this section are R_L is the equivalent load resistance of the rectifier and the battery load, R_1 is the resistance of the coil L_1, whereas R_2 is the resistance of the coil L_2, P_1 is the power generated at the primary side, P_2 is the power transferred to the secondary side, M is the mutual inductance, V_1 is the voltage source, I_1 is the current at primary side and f is the frequency [9].

The efficiency can be calculated by

$$\eta = \frac{P_2}{P_1} \qquad (2-27)$$

The power at the primary side can be obtained as

$$P_1 = \frac{{V_1}^2}{R_1 + \frac{\omega^2 M^2}{R_2 + R_L}} \qquad (2-28)$$

And the power at the secondary side can be obtained by

$$P_2 = \frac{\omega^2 M^2 {I_1}^2}{R_L} \qquad (2-29)$$

Where ω is the resonant frequency of the primary and secondary [8], it is normally chosen by

$$\omega = \frac{1}{\sqrt{L_1 C_1}} = \frac{1}{\sqrt{L_2 C_2}} \qquad (2-30)$$

And can be calculated by

$$\omega = 2\pi f \qquad (2-31)$$

CHAPTER 3

MATLAB Code Calculations

And

Model Simulation Results

In this chapter Matlab codes calculations in section 3.1 and Matlab simulation model in section 3.2 were used to calculate and obtain the parameters of the designed system. Charging battery of a laptop 20 Volts at 6 Amps (120 Watts Power) has an equivalent resistive load of 3.3 Ω.
For this purpose the design was made and the results were compared.

3.1 Parameters Calculations using Matlab Codes

3.1.1 Matlab Code 1 Calculations

Code 1 is used to obtain the theoretical values of the inductance $\mathbf{L_1}$ and $\mathbf{L_2}$, the mutual inductance **M**, the resistance of the coils $\mathbf{R_1}$ and $\mathbf{R_2}$, the series capacitors $\mathbf{C_1}$, $\mathbf{C_2}$ and the coupling coefficient **k** (Code 1 is attached in appendix A)

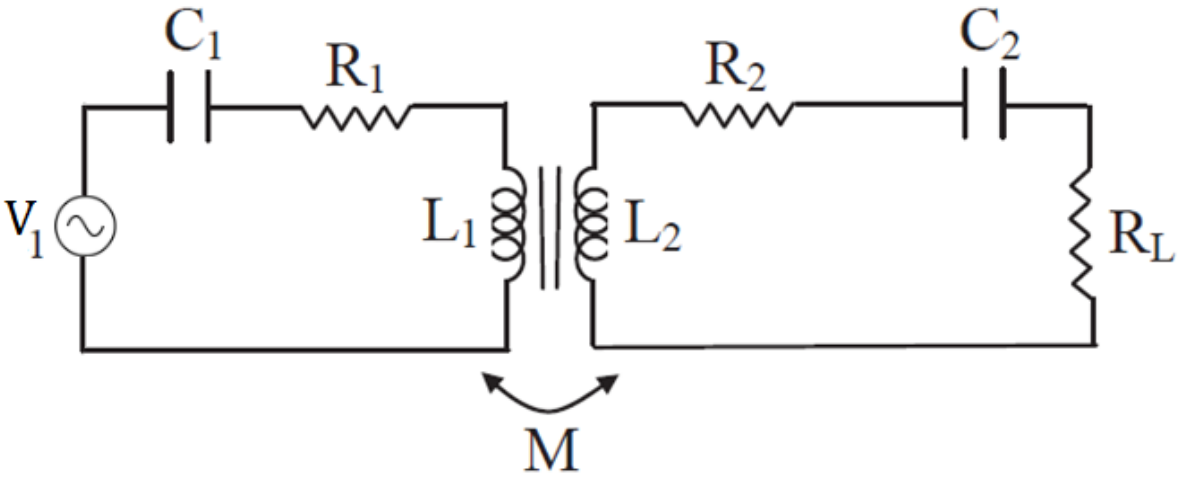

Fig 3.1 Scheme of the implemented model and theoretical parameters

The input values for the desired design are

Table 3.1 Input values of code 1

Parameters	**Input**
L Length of primary coil	0.45 M
A Length of secondary coil	0.1 M
D Width of primary and secondary coils	0.25 M
H Height	0.03 M
N1 Number of turns for coil 1	12
N2 Number of turns for coil 2	12
S1 Section of the Litz-wire windings	10e-6
S2 Section of the Litz-wire windings	30e-6
u0 Permeability of the air	$4\pi 10^{-7} H.m^{-1}$
F Frequency	18 KHz

The calculated output values are

Table 3.2 Output values of code 1

Parameters	**Calculated**
L1 Inductance of the primary winding	138.47 µH
L2 Inductance of the secondary winding	41.98 µH
C1 Capacitor 1 for primary coil	0.564 µF
C2 Capacitor 2 for secondary coil	1.862 µF
R1 Primary coil resistance	0.2947 Ω
R2 Secondary coil resistance	0.0491 Ω
M Mutual inductance	12.254 µH
k Coupling coefficient	0.1607

3.1.2 Matlab Code 2 Calculations

When applying the output parameters of code 1 in additional to the new inputs of code 2 we obtain from **Code 2** the calculated theoretical values of the primary circuit and they are the current at primary side is $\mathbf{I_1}$, the power generated in primary side $\mathbf{P_1}$

The parameter of the secondary circuit are the voltage $\mathbf{V_2}$, The current at secondary side $\mathbf{I_2}$, the power transferred from primary to secondary side $\mathbf{P_2}$, the equivalent load resistance **RL**, the terminal load **RLoad**, the total impedance of the secondary side of the circuit $\mathbf{Z_2}$, the total impedance of the primary and secondary sides **Ztotal**, And the efficiency of the system **η**
(Code 2 is attached in appendix A)

The input values for the desired design are

Table 33 Input values of code 2

Parameters	**Input**
V1 Inverter output voltage	17 V
VLoad Desired output DC voltage at terminal load	20 V
ILoad Desired output current at terminal load	6 A

The output values are

Table 3.4 Output values of code 2

Parameters	Calculated
RLoad Terminal load	3.3333 Ω
N Transformer turn ratio	1
RL Equivalent load resistance	2.70 Ω
Z2 Total impedance of secondary side	2.75 Ω
Ztotal Total impedance all circuits	0.992 Ω
I1 Inverter output current	17.1 A
I2 Load current	8.62 A
V2 Load voltage	26.5 V
P1 Power generated in primary side	291 W
P2 Power output at secondary side	168.9 W
η Efficiency = P2/P1	58 %

3.2 Circuit Analysis and Simulation in Matlab

In this section the calculated values of the previous Matlab codes 1 and 2 were applied to the simulation model in Matlab. The simulated parameters values are shown in the next tables and scopes photos.

3.2.1 Schematic Circuit Diagram

Fig 3.2 shows the scheme of the simulated model in Matlab. The measurements for the voltage and current and were taken from 4 different sections.

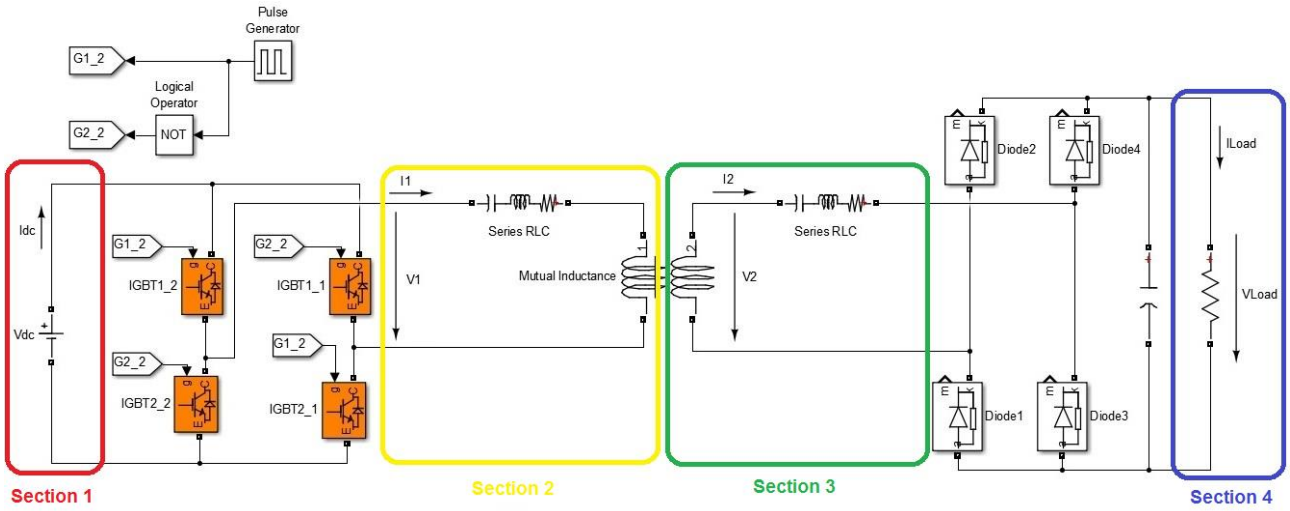

Fig 3.2 Scheme of the implemented model in Matlab

3.2.2 Simulated model results and comparisons

From the schematic circuit in Fig 3.2 it will be split for 4 sections on each section there will be acquired (voltage, current and power) The DC input voltage for the IGBTs inverters Vdc is 17V.

Note: Matlab Code 1 and Code 2 only calculate the parameters for the sections yellow and green in Fig 3.2

Section 1: At the primary DC circuit (Red Section)

Table 3.5 shows the simulated Mean values of voltage, current and power at section 1 of Fig 3.2

Table 3.5 Simulated Mean values for Vdc, Idc and Pdc at the primary DC circuit

Parameters on 1st Section	Simulated	Calculated
Vdc Voltage mean value	17 V	-
Idc Current mean value	14.3 A	-
Pdc Power value	243 W	-

The scopes in Fig 3.3 display the generated signals of the simulated instantaneous values for vdc in blue color, idc in green color and pdc in red color. It can be seen that the voltage vdc is ideal source.

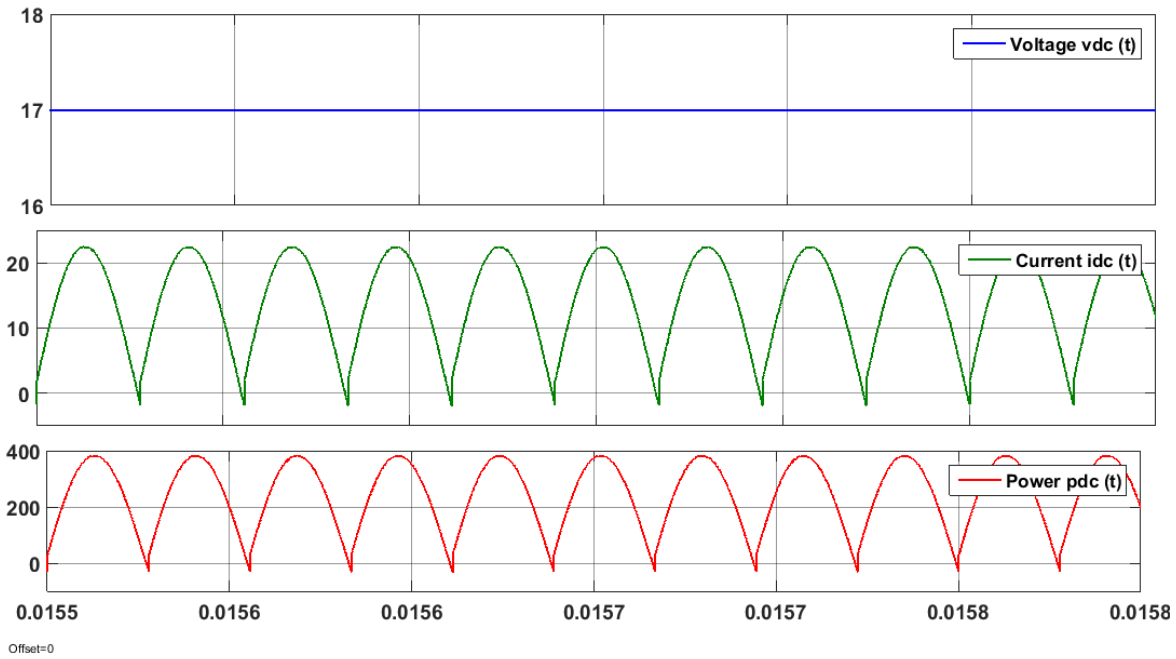

Fig 3.3 Simulated instantaneous values for vdc, idc and pdc at the primary DC circuit

Section 2: At the primary AC circuit (Yellow section)

Table 3.6 shows the simulated and calculated RMS values of voltage, current and power at section 2 of Fig 3.2

Table 3.6 Comparison for the RMS values of V1, I1 and P1 at the primary AC circuit

Parameters on 2nd Section	Simulated	Calculated
V1 Voltage RMS value	16.97 V	17 V
I1 Current RMS value	15.94 A	17.12 A
P1 Power value	242 W	291 W

The first scope in Fig 3.4 displays the simulated instantaneous values of v1 and i1 at the primary AC circuit. It can be seen that the current have perfect sine wave. Here the voltage and current are working at resonance frequency (fs=18000Hz = fr=18000Hz) and have zero phase angle $\theta = 0°$ The circuit operates on the inductive region switching (ZVS) that mean it achieve the maximum output power with the minimum input VA rating. The second scope displays the simulated instantaneous value for the p1 at the primary AC circuit which is the product of the corresponding instantaneous values of v1 and i1.

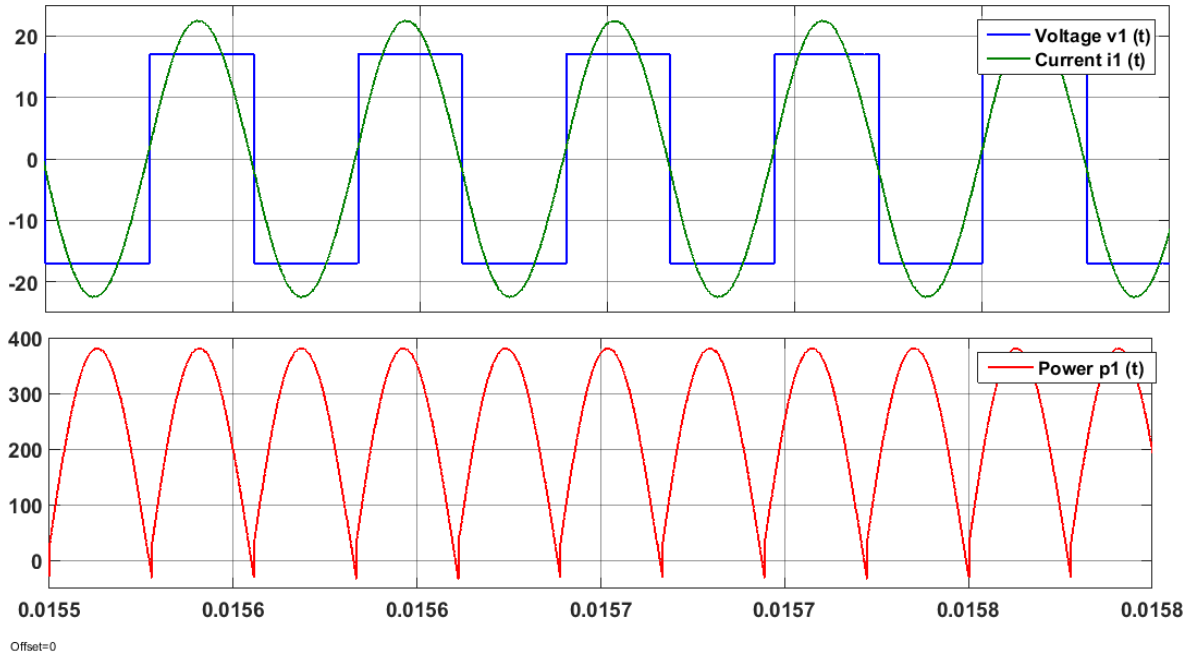

Fig 3.4 Simulated instantaneous values for the v1, i1 and p1 at the primary AC circuit

Section 3: At the secondary AC circuit (Green section)

Table 3.7 shows the simulated and calculated RMS values of voltage, current and power at section 3 of Fig 3.2

Table 3.7 Comparison for the RMS values of V2, I2 and P2 at the secondary AC circuit

Parameters on 3rd Section	**Simulated**	**Calculated**
V2 Voltage RMS value	22.1 V	26.5 V
I2 Current RMS value	7.67 A	8.6 A
P2 Power value	167 W	168 W
η Efficiency = P2/P1	69 %	58 %

The first scope in Fig 3.5 displays the simulated instantaneous values of v2 and i2 at the secondary AC circuit. Here the voltage and current are also working at resonance frequency (fs=18000Hz = fr=18000Hz) and have zero phase angle $\theta = 0°$ The circuit operates on the inductive region switching (ZVS). The second scope displays the simulated instantaneous value for the power p2 at the secondary AC circuit. The power transferred from the primary coil to the secondary coil is maximum because the operation mode is at resonance.

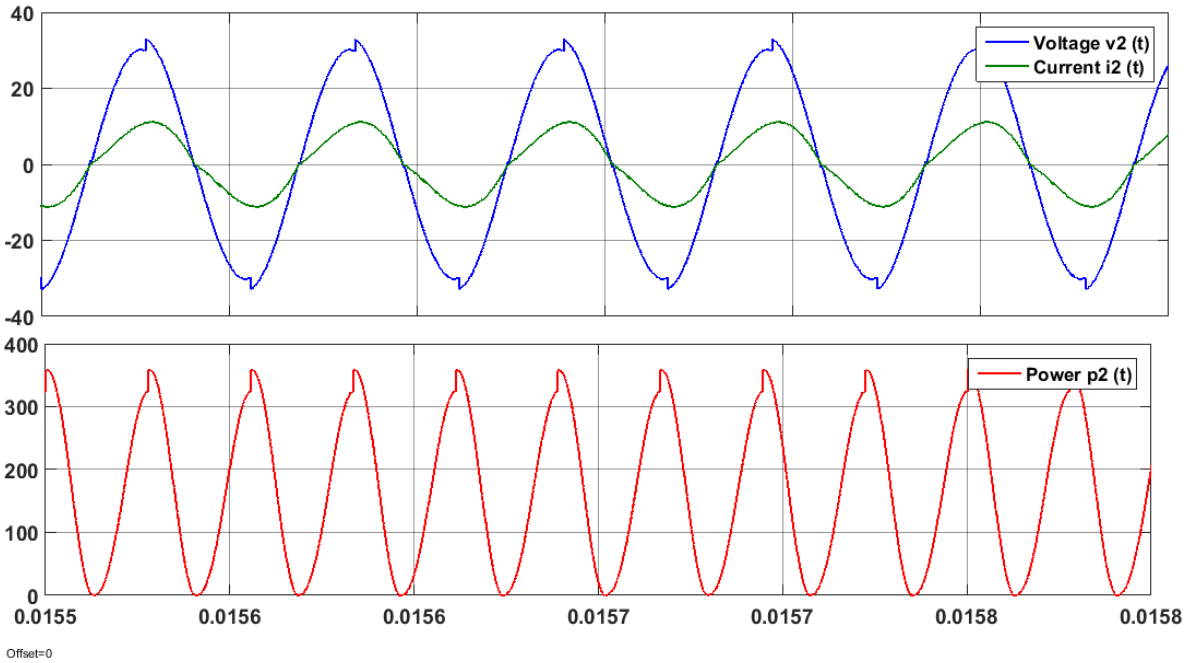

Fig 3.5 Simulated instantaneous values for v2, i2 and p2 at the secondary AC circuit

Section 4: At the secondary DC circuit (Blue section)

Table 3.8 shows the simulated and calculated Mean values of voltage, current and power at section 4 of Fig 3.2

Table 3.8 Simulated Mean values for Vload, Iload and Pload at the secondary DC circuit

Parameters on 4th Section	**Simulated**	**Calculated**
Vload Voltage Mean value	22.5 V	-
ILoad Current Mean value	6.76 A	-
Pload Power value	152 W	-
η Efficiency of the system = Pload/Pdc	62 %	-

The scope In Fig 3.6 displays the generated signals of the simulated instantaneous values for vload in blue color, iload in green color and pload in red color. It can be seen that the ripples on both voltage and current waveforms are small.

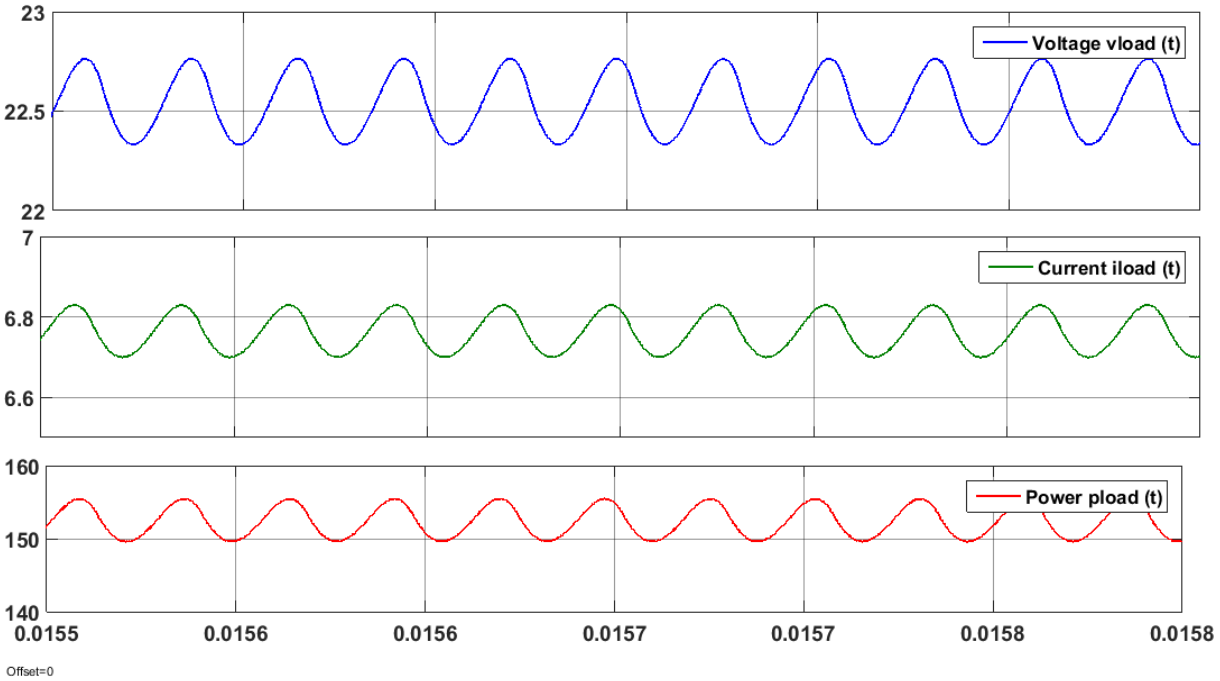

Fig 3.6 Simulated instantaneous values for vload, iload and pload at the secondary DC circuit

CHAPTER 4

Laboratory Experiment and Results Comparison

In this chapter the design of the previous chapter 3 Charging battery of a laptop 20 Volts at 6 Amps (120 Watts Power) was not possible to be applied in the laboratory due to the limitation of the power supply to 5 Amps. For this reason a different lower design was experimentally implemented and compared with its own calculated and simulated results.

4.1 System Design

The experimental circuit at the primary side contains the DC power supplies for the isolation board and the IGBTs inverters managed by a driving DSP board which generate PWM signals followed by the isolation board followed by the primary coil L1 and the compensation C1.

The circuit at secondary side contains the secondary coil L2 and the compensation C2 followed by the rectifiers and the terminal load at the end. In this system the capacitors are in series with the inductors to set to the resonant frequency.

The two circuits need to resonate at the same frequency in order to function properly and achieve maximum output power at the minimum input VA rating. It is important to note that resonance increases the range of wireless power transfer.

The algorithm was presented in chapter 3 and was used to calculate the values of the capacitors C1 and C2 for the measured inductors L1 and L2 by the LCR meter at frequency of 18182Hz. this will allow the circuit to operate at resonance and draw the maximum efficiency.

As a result the system was designed. Measurements and calculation were made in the build setup in order to obtain the mutual inductance value at 3 cm height. The experimental system in Fig 4.1 is compared with its simulated and calculated models in Matlab.

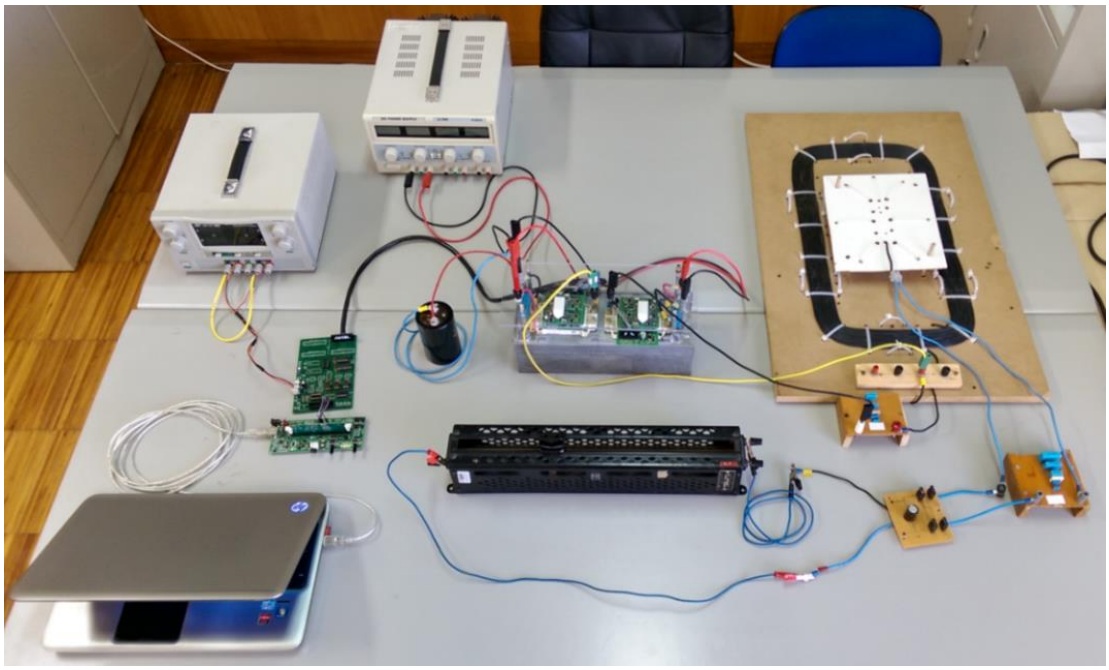

Fig 4.1 Experimental wireless power transfer system setup

4.2 Transmitter Equipment

4.2.1 DSP Board

The DSP board in Fig 4.2 is made by Texas Instruments, has TMS320F28335 control card generates the desired PWM pulses, the frequency set for this project is 18182 Hz, a square wave driving the inverters after the signals have been amplified in the isolation board, the DSP board is USB powered and can be externally powered to support other types of uses, it can be programed by Matlab in additional to its original code composer studio software.

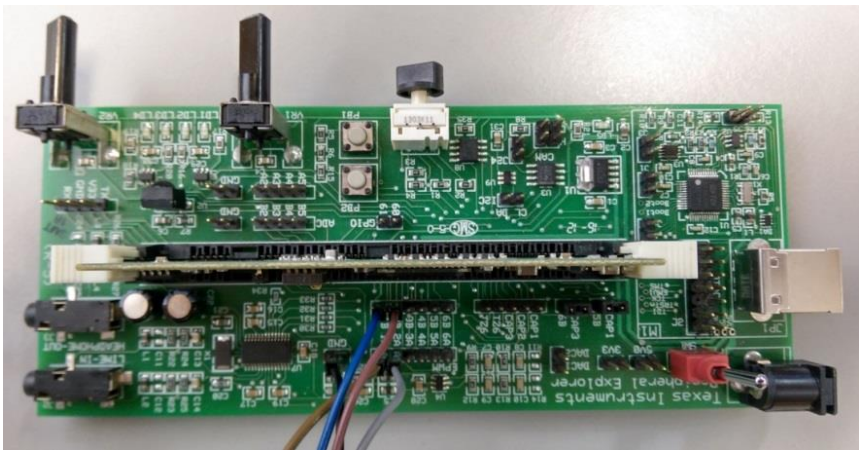

Fig 4.2 DSP board Texas instrument F28335

4.2.2 Isolation Board

The main role of the isolation board in Fig 4.3 is to amplify and isolate the signals coming from the DSP board, it amplifies the voltage from 3.3V (DSP board) to 15V (inverters board), two dual digital isolators were placed between the gate driver and the DSP for each inverter leg.

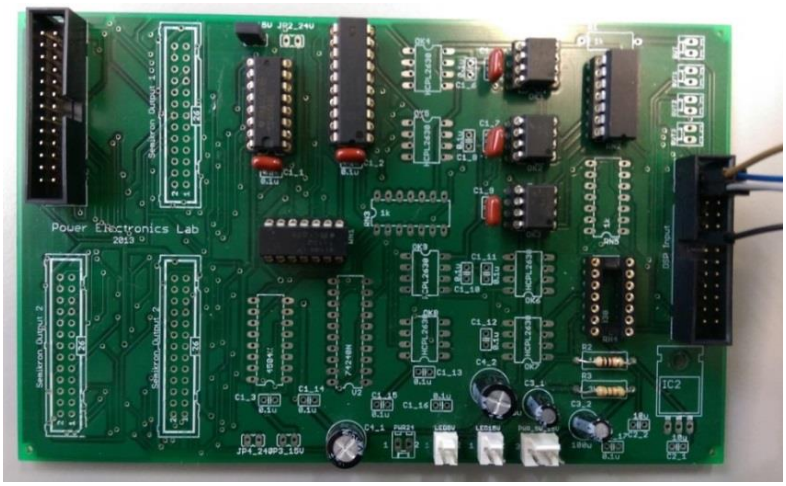

Fig 4.3 Isolation board

4.2.3 Connection Cables

There are two cables, one as shown in Fig 4.4 for connecting the DSP board to the isolate board and the second as shown in Fig 4.5 cable for connecting the isolation board to the two inverters boards (each inverter board has two IGBTs inverters) Table 4.1 and 4.2 explain the connected input and output pins of each board socket.

Table 4.1 DSP board output pins to isolation board input pins

DSP Board Output	From Pin	Isolate Board Input	To Pin
Data 1	1A	Data 1	1
Data 2	1B	Data 2	2
Data 3	2B	Data 3	3
Data 4	2A	Data 4	4
GND	GND 1	GND	11

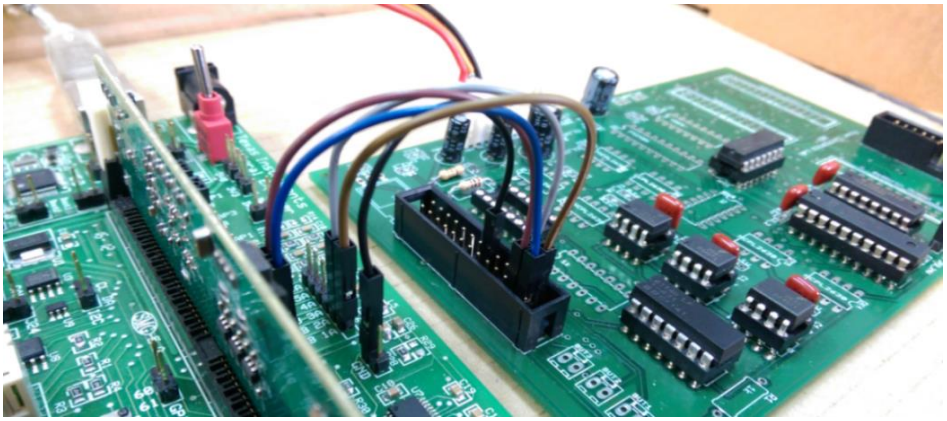

Fig 4.4 DSP to isolation board wires (5x1 Pin to Pin)

Table 4.2 Isolation board output pins to inverters boards input pins

Isolate board Output	From Pin	IGBTs board 1 Input	To Pin	IGBTs board 2 Input	To Pin
Data 1	2	Data Top Switch	15	-	-
Data 2	4	Data Bot Switch	16	-	-
GND 1	8	GND	6	-	-
15V 1	16	15V	3	-	-
Data 3	5	-	-	Data Top Switch	15
Data 4	7	-	-	Data Bot Switch	16
GND 2	10	-	-	GND	6
15V 2	15	-	-	15V	3

Fig 4.5 Isolate board to inverters boards (Y Cable 26 pins socket to 2x20 pins sockets)

4.2.4 Isolation board's Power supply

This power supply in Fig 4.6 converts the standard 230V 50 Hz AC to up to 30V DC at 5A maximum. It outputs sets to 5V DC and 15V DC. The 5V used for the ICs complements of the isolation board and the 15V used for amplifying the 3.3V PWM signals from the DSP, because the input of voltage for the IGBTs inverters required 15V DC to function.

Fig 4.6 Isolation board power supply

4.2.5 IGBTs Power supply

The power supply in Fig 4.7 provides appropriate voltage and current levels for the high and low side transistors of the inverters, it converts 230V 50Hz AC to up to 30V DC at 5A Max.

Fig 4.7 IGBTs power supply

4.2.6 H-Bridge Transistors

An H-bridge is a configuration of four IGBTs transistors. the type used in this project is SKYPER 32 PRO by SIMIKRON as shown in Figure 4.11 the outputs ports of the transistors are connected to both sides of the primary coil and the primary series capacitor, by alternating the switching of opposing pairs of transistors, the H-bridge is able to reverse the current flow through the primary coil, simulating an AC source. Each piece of the two contains two IGBSs transistors.

The only downside of these transistors is the operating frequency, they doesn't support more than 20 KHz and for wireless power transfer when working on higher frequency will result to better system efficiency for the same design. MOSFETs transistors were preferred but due to the non-availability in the laboratory I had to use the IGBTs transistors.

4.2.6.1 Preparing the IGBTs Transistors boards

There are set of resistors and one capacitor was used to build each transistors board Table 4.3 describe the components values used for each board. Fig 4.8 to Fig 4.11 explains the preparation steps.

Table 4.3 Components used for each IGBTs board

Type of Competent	Quantity	Value
Resistor	1	820 Ω
Resistor	4	4 Ω
Resistor	12	5.7 Ω
Resistor	2	0 Ω
Resistor	2	18 kΩ
Capacitor	2	330 pF

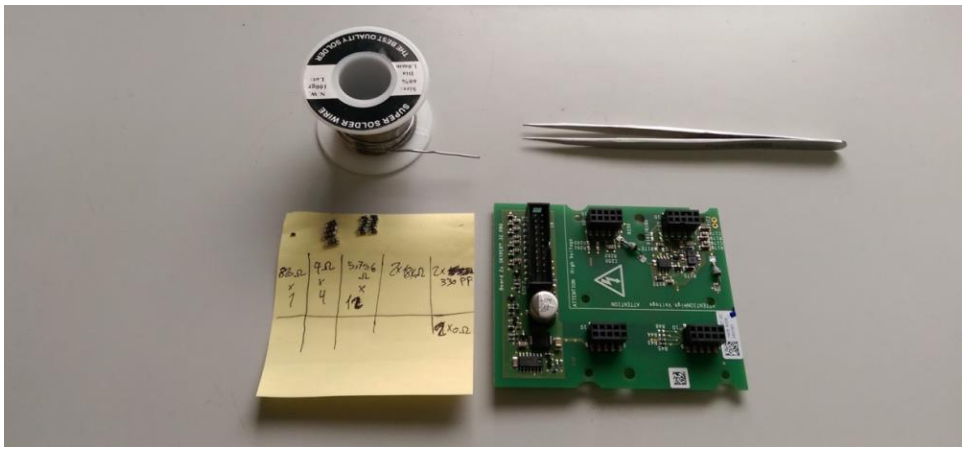

Fig 4.8 Soldering the components on the board

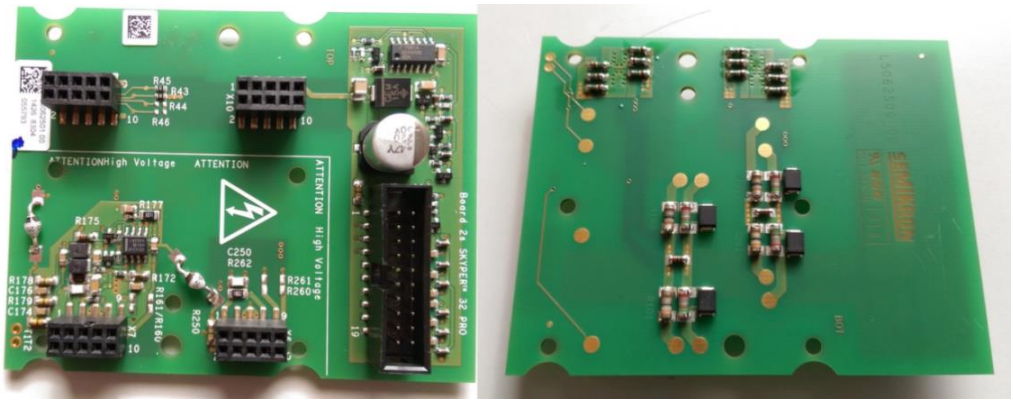

Fig 4.9 Board is ready from front and back sides

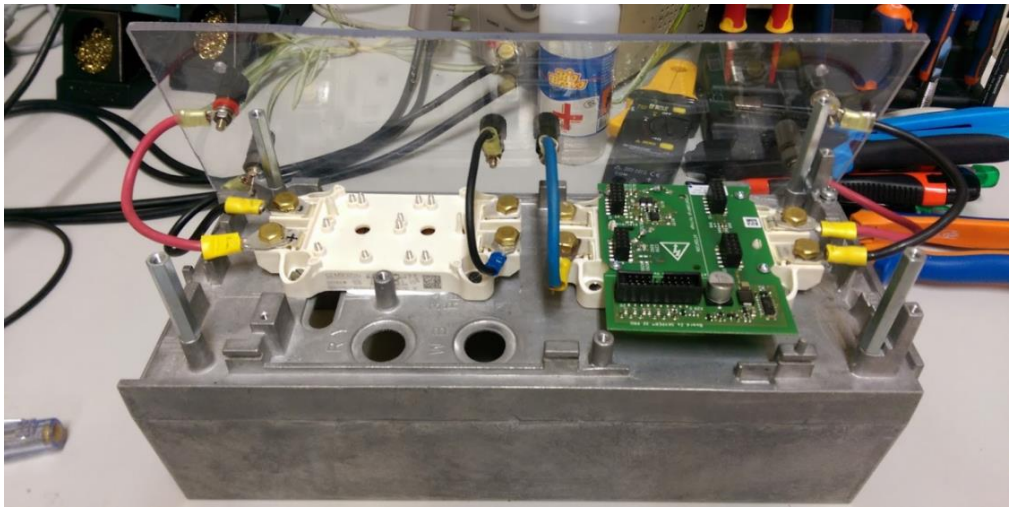

Fig 4.10 Installing the IBGTs boards on the chasse

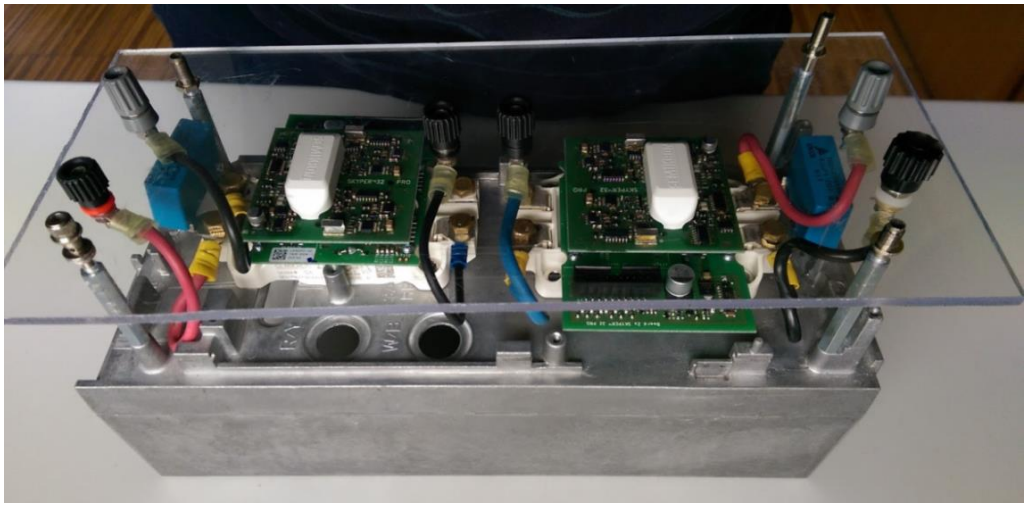

Fig 4.11 H-Bridge inverters are ready after adding the snubber capacitors

4.2.7 PWM Setup

The PWM module generates the PWM signal to the 4 IGBTs inverters. The signal for the two IGBTs in one inverter leg is the complimentary of each other, which mean when the upper IGBT is on the lower IGBT is off and vice versa.

Matlab were used to build the blocks and then flash it to the DSP board to set the switching frequency to 18182 Hz.

Fig 4.12 shows the Matlab model of PWM pulse generator for 4 IGBTs inverters.

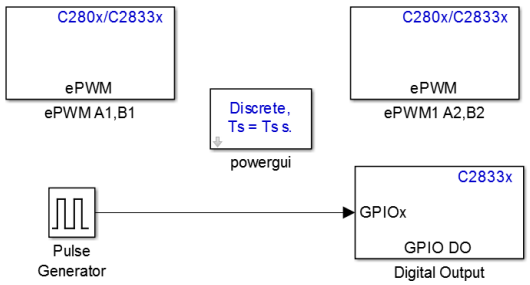

Fig 4.12 PWM pulse generator for 4 IGBTs inverters

4.2.8 Transmitter Coil

The primary coil used in this project was prepared previously from an old project, the cable used in it have a 3mm wire diameter and 12 turns as shown in Fig 4.13, it is wired in series with a capacitor such that they both have a resonant frequency f=18182 Hz, the measured inductance L1 and resistance R1 from the LCR meter at this frequency are L1=94.66 µH, R1=0.55 Ω and The calculated resonance capacitor for this frequency is C1=809.4nF, to find the exact value of this capacitor is hard, the solution was to combine multiple capacitors and wire them together in parallel to achieve the closest value possible. C1 was combined by 5 capacitors from different sizes have an experimental measured value C1=783 nF as shown in Fig 4.14.

By applying the average dimensions of the experimental rectangular primary coil in Matlab Code1, the results are L1=94.77µH, R1=0.30Ω this indicate that the equation used to calculate the self-inductance to be valid for planar coils with multiple numbers of turns.

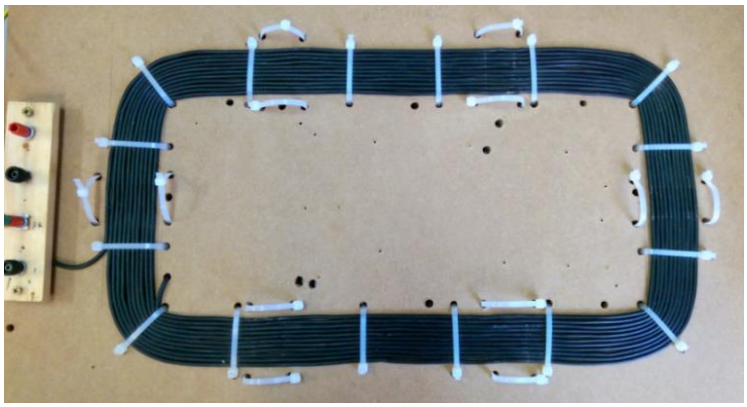

Fig 4.13 Transmitter coil at primary side

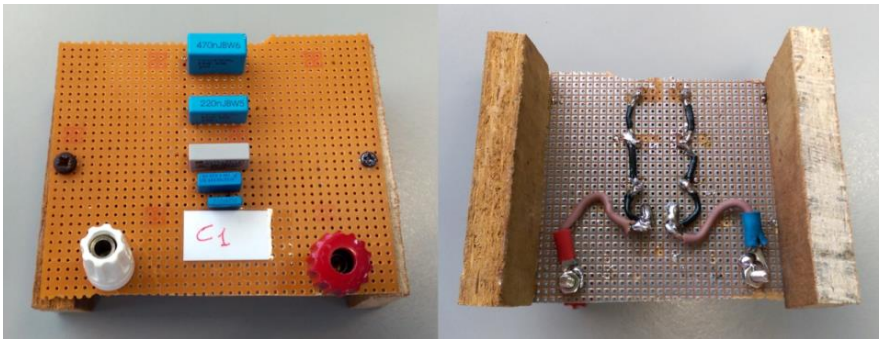

Fig 4.14 Transmitter coil equivalent series capacitor at primary side

4.3 Receiver Circuit

The main purpose of the receiver circuit is to transfer the power created by the transmitter magnetic field to the system/battery. In order for this circuit to work properly, there are two stages, the first one is to convert the AC input voltage to a steady DC voltage by the rectifier and the second stage is to store the energy collected from the transfer side to a system/battery. Fig 4.15 and Fig 4.16 presents an overview of the components used in order to achieve the desired voltage and current to power.

4.3.1 Receiver Coil

The secondary coil used in this project was prepared previously from an old project, the cable used in it have a 3mm wire diameter and 12 turns as shown in Fig 4.15, it is wired in series with a capacitor such that they both have a resonant frequency f=18182Hz, the measured inductance L2 and resistance R2 from the LCR meter are L2=21.73µH, R2=0.047Ω the calculated resonance capacitor for this frequency is C2=3526nF, to find the exact value of this capacitor is hard, the solution was to combine multiple capacitors and wire them together in parallel to achieve the closest value possible. C2 was combined by 6 capacitors from different sizes and have an experimental measured value C2=3700nF as shown in Fig 4.16

By applying the average dimensions of the secondary experimental rectangular coil in Code 1, the results are L2=21.8 µH, R2=0.1 Ω this indicate that the equation used to calculate the self-inductance to be valid for planar coils with multiple numbers of turns.

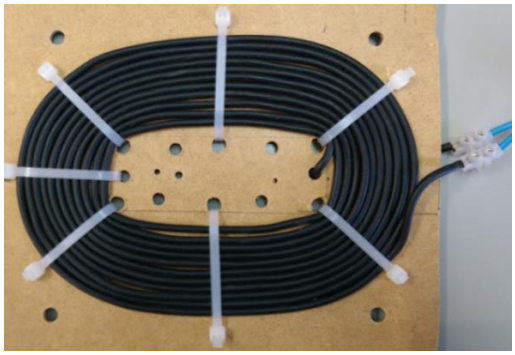

Fig 4.15 Receiver coil at secondary side

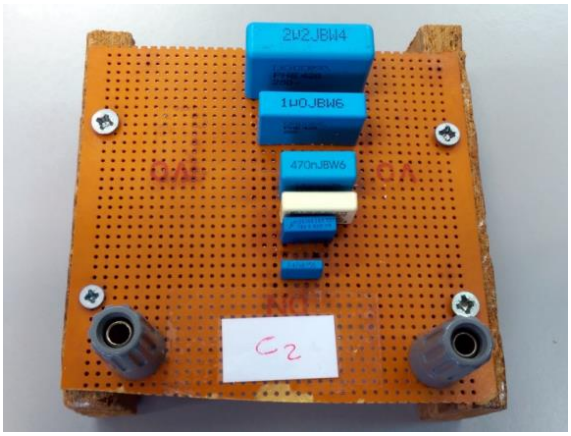

Fig 4.16 Receiver coil equivalent series capacitor at secondary side

4.3.2 Rectifier

A rectifier is an electrical device that converts alternating current AC, which periodically reverses direction, to direct current DC, which flows in only one direction. The process is known as rectification. Physically, reciters take a number of forms, including solid-state diodes, silicon-controlled rectifiers and other silicon-based semiconductor switches [18]. A full-wave bridge rectifier is an arrangement of four diodes in a bridge circuit configuration that provide a desired output, The essential feature of a full-wave bridge rectifier is that the polarity of the output is the same regardless of the polarity at the input. The operation of the bridge rectifier is as follows:

1. In the positive half cycle of the AC sine wave signal, diodes D1 and D2 are in forward bias and will conduct while diodes D3 and D4 are reverse biased. The current will flow through diodes D1 and D2.
2. In the negative half cycle, diodes D1 and D2 are now in reverse biased.

Rectifier have high frequency response was needed to operate at this frequency f=18182 Hz

I had to build the rectifiers circuit which made by 4 diodes type 80EPF12, and the capacitor were calculated and the approximate value where used C=47 µF. Fig 4.17 shows the rectifier used.

$$C = \frac{I\ t}{\Delta \mathrm{V}} \qquad (4-1)$$

Where:

C is the capacitance in farads

I is the DC load current in amperes

t is the period of the full-wave rectified waveform, in seconds

ΔV is the ripple across the allowable load, in volts

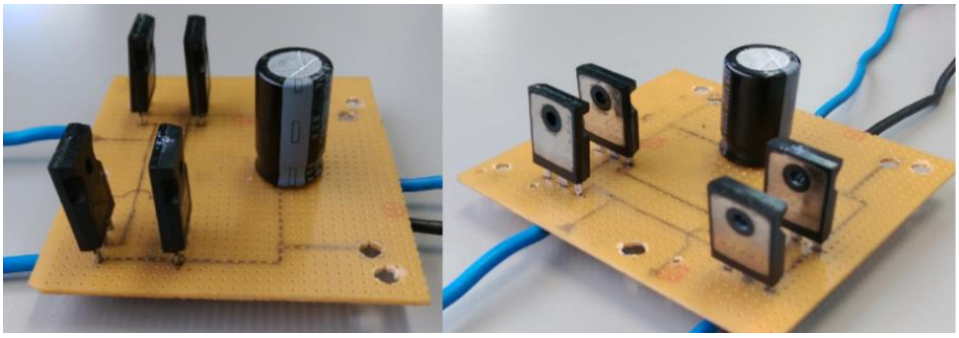

Fig 4.17 High frequency AC-DC full bridge rectifier

4.3.3 Load

Fig 4.18 show the variable resistances at the terminal load where used and set to a value of 1.9 Ω

Fig 4.18 Terminal RLoad

4.4 Experimental Results

4.4.1 Parameters of the system

As seen in Table 4.4 some parameters of the experimental circuit were measured by LCR meter and the other parameters were obtained from Matlab Code 1 and Code 2 depending on the measured values of the LCR meter, the input voltage of the IGBTs inverters is 6V at maximum because the power supply doesn't supply more than 5 amps. The calculated and experimented values for the inductance L_1, L_2 and the resistance of the coils Res_1, Res_2 and the capacitors C_1, C_2 are shown in Table 4.4 but only the experimental values were used in the simulation to be comparable with the experimental results (Matlab codes used for this simulation are attached in appendix B)

The primary coil and the second coil with the combined capacitors C1 and C2 are working on different modes of operation this because the capacitors C1 and C2 doesn't have the same exact values as the calculated values of Code 1, in result this will affect the power transfer capability of the system.

The phase angle between the voltage and current is obtained by

$$\theta = Cos^{-1}\left(\frac{P}{V\,I}\right) \qquad (4-2)$$

The experimental mutual inductance value between the coils where obtained by

$$M = \frac{V2}{\omega\, I1} \quad = \quad \frac{V1}{\omega\, I2} \qquad (4-3)$$

Table 4.4 Parameters of the experimental model

Parameters	Experimented	Calculated	Selected
Vdc IGBTs input Voltage	-	-	6 V
f Frequency	18182 Hz	-	-
L1 Inductance of the primary winding	94.66 µH	94.77 µH	-
L2 Inductance of the secondary winding	21.73 µH	21.8 µH	-
Res1 Primary Coil Resistance	0.55 Ω	0.30 Ω	-
Res2 Secondary Coil Resistance	0.047 Ω	0.10 Ω	-
RLoad Terminal Load	-	-	1.9 Ω
RL Equivalent load resistance in AC circuit	-	1.540 Ω	-
Ztotal Total impedance	-	0.940 Ω	-
Z2 Equivalent load impedance of secondary side	-	1.591 Ω	-
C1 Capacitor 1 for primary coil	783 nF	809.4 nF	-
C2 Capacitor 2 for secondary coil	3700 nF	3526 nF	-
M Mutual inductance	6.12 µH	-	-

4.4.2 Experimental model results and comparisons

As seen from Fig 3.2 the measurements were taken at 4 different sections from the schematic circuit. The experimented results were compared with the simulated and the calculated values.

Note: Matlab Codes 1 and Code 2 only calculate the parameters of section 2 in yellow and section 3 in green from Fig 3.2

Section 1: At the primary DC circuit (Red section)

Table 4.5 shows the experimented, simulated and calculated values of voltage, current and power at section 1 of Fig 3.2

Table 4.5 Comparison for the Mean values for Vdc, Idc and Pdc at the primary DC circuit

Parameters on 1st Section	Experimented	Simulated	Calculated
Vdc Voltage Mean value	6 V	6 V	-
Idc Current Mean value	4.78 A	5A	-
Pdc Power value	28.3 W	30 W	-

The screen of the oscilloscope in Fig 4.19 display the generated signals of the experimental instantaneous values of vdc in yellow color, idc in blue color and pdc in red color. It can be seen that the output voltage idc of the power supply is not pure DC Voltage because it is not originate from ideal DC source.

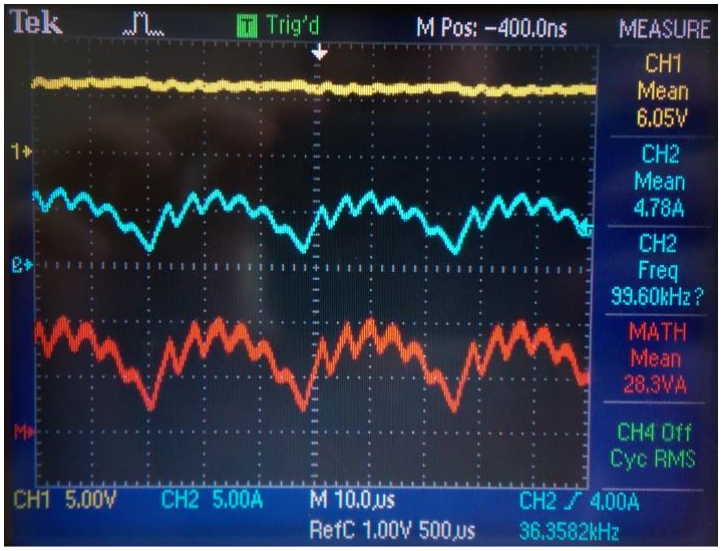

Fig 4.19 Experimental instantaneous values for vdc, idc and pdc at the primary DC circuit

The scopes in Fig 4.20 display the generated signals of the simulated instantaneous values for vdc in blue color, idc in green color and pdc in red color.

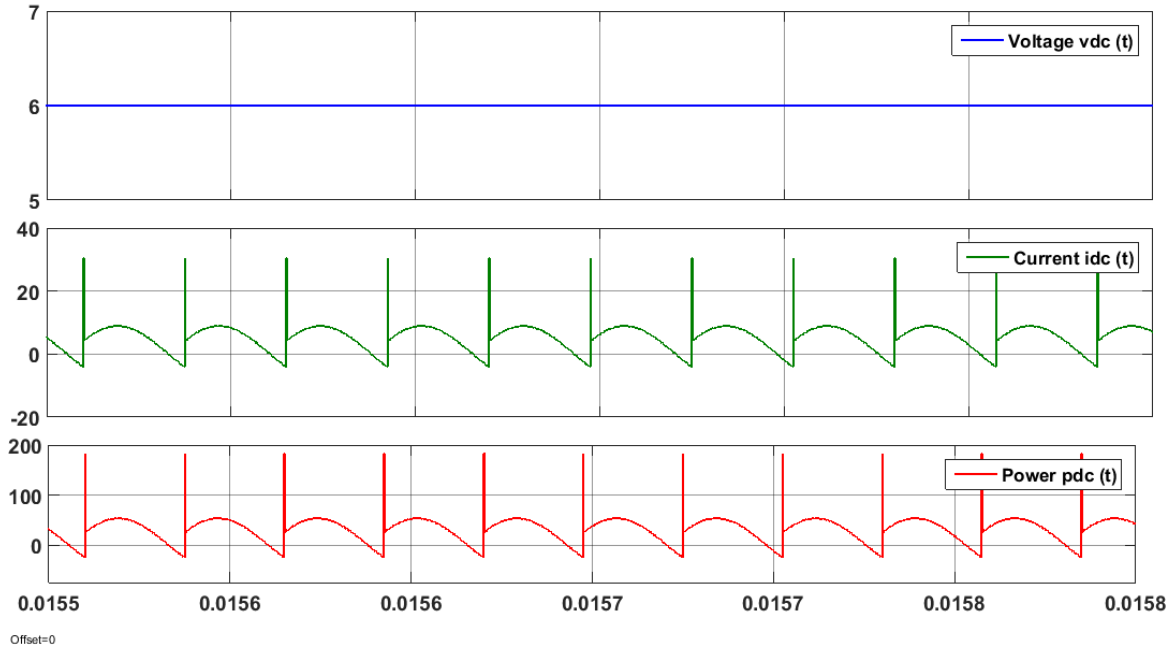

Fig 4.20 Simulated instantaneous values for vdc, idc and pdc at the primary DC circuit

Section 2: At the primary AC circuit (Yellow section)

Table 4.6 shows the experimented, simulated and calculated RMS values of voltage, current and power at section 2 of Fig 3.2

Table 4.6 Comparison for the RMS values for V1, I1 and P1 at the primary AC circuit

Parameters on 2nd Section	Experimented	Simulated	Calculated
V1 Voltage RMS value	4.69 V	5.99 V	6 V
I1 Current RMS value	4.95 A	6.25 A	6.38 A
P1 Power value	17.9 W	29.4 W	30.8 W

In figure 4.21 the screen of the oscilloscope display the generated signals of the experimental instantaneous values for v1 in yellow, i2 in blue and p1 in red at the output of the full bridge inverters in the primary AC circuit.

In both Fig 4.21 and Fig 4.22 we can see the current is almost perfect sine wave for the experimental and simulation. In Fig 4.21 it can be seen there is a small difference in phase shift between v1 and i1, the shifting angle were calculated from equation (4-2) and it is $\theta = 41.5°$ this shifting is because of the combined capacitors in C1 have a smaller value than the calculated one. The switching frequency is lower than the operation frequency of L1+C1 (fs=18182Hz < fr=18486Hz) that means it's working below the resonant frequency on the capacitive region (ZCS) zero current switching. This will not achieve the maximum output power at the minimum input VA rating at the transmitter stage.

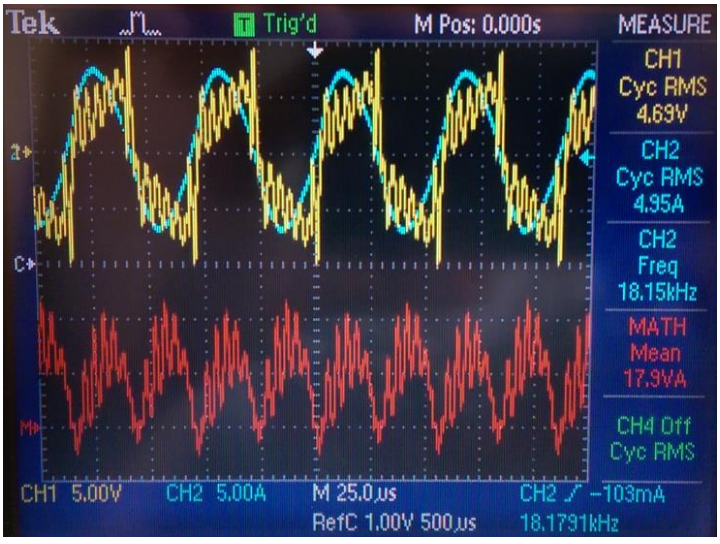

Fig 4.21 Experimental instantaneous values for v1, i1 and p1 at the primary AC circuit

The first scope in Fig 4.22 displays the simulated instantaneous values of v1 and i1 at the primary AC circuit. It can be seen there is a small difference in phase shift between v1 and i1,

the shifting angle is $\theta = 33.5°$ it's also working below resonant frequency on the capacitive region (ZCS). The second scope in Fig 4.22 displays the simulated instantaneous value for p1 at the primary AC circuit.

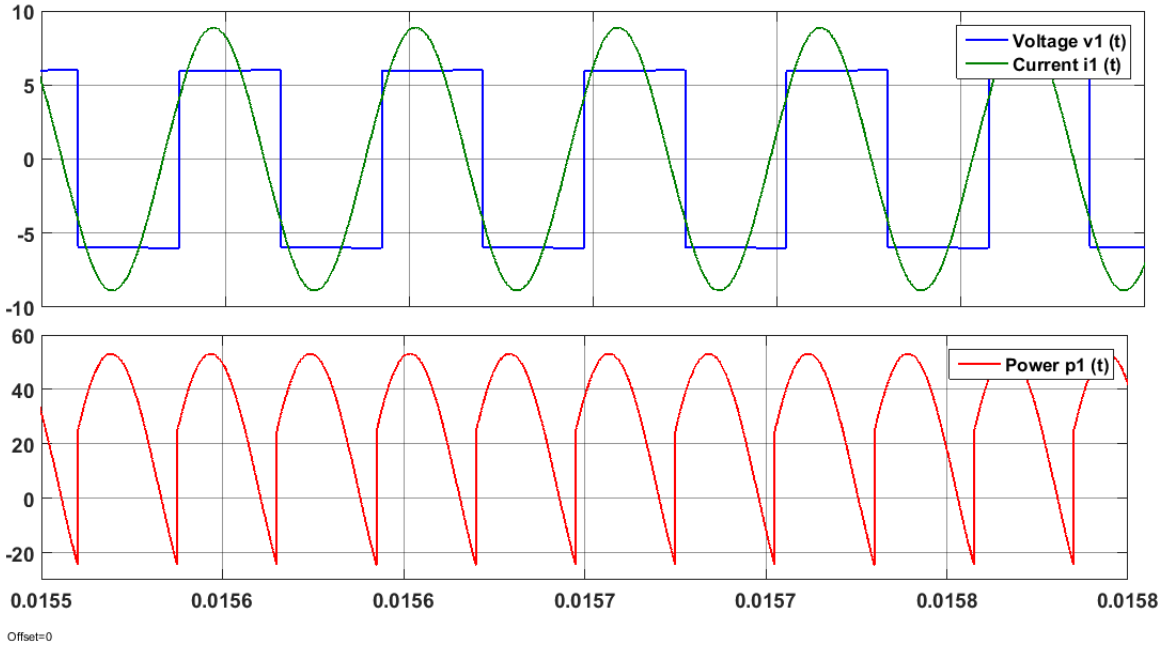

Fig 4.22 Simulated instantaneous values for v1 and i1 at the primary AC circuit

Section 3: At the Secondary AC Circuit (Green Section)

Table 4.7 shows the experimented, simulated and calculated values of voltage, current and power at section 3 of Fig 3.2

Table 4.7 Comparison for the RMS values of V2, I2 and P2 at the secondary AC circuit

Parameters on 3rd Section	**Experimented**	**Simulated**	**Calculated**
V2 Voltage RMS value	5.05 V	4.37 V	4.74 V
I2 Current RMS value	1.6 A	1.8 A	2.8 A
P2 Power value	5.83 W	7.95 W	10.4 W
η Efficiency = P2/P1	33.8 %	27 %	34 %

In Fig 4.23 the screen of the oscilloscope display the generated signals of the experimental instantaneous values for v2 in yellow, i2 in blue and P2 is in red at the secondary AC circuit in the secondary coil. It can be seen there is a small difference in phase shift between v2 and i2, the shifting angle is $\theta = 43.8°$ this because of the combined capacitors in C2 have a bigger experimental value than the calculated value because of this, the switching frequency is higher than the operation frequency of L2+C2 (fs=18182Hz > fr=17749Hz) this means we are working above the resonant frequency and the operation working region is on the inductive region switching (ZVS).

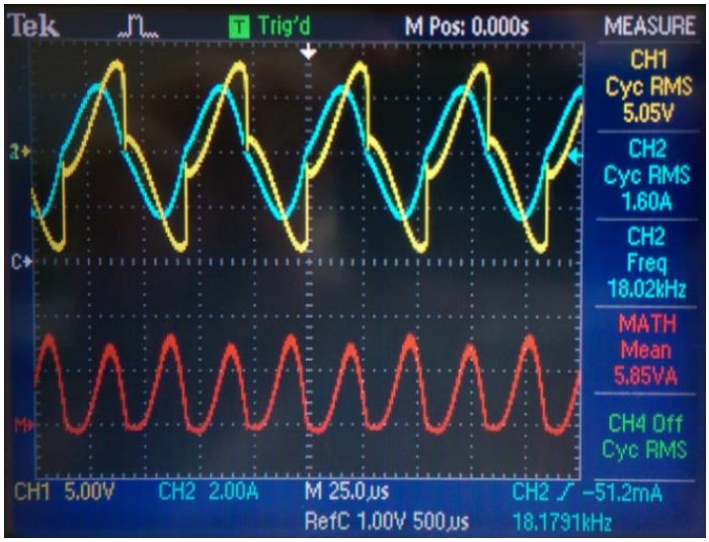

Fig 4.23 Experimental instantaneous values for v2, i2 and p2 at the secondary AC circuit

The first scope in Fig 4.24 displays the simulated instantaneous values of v2 and i2 at the secondary AC circuit. When applying equation (4-2) it shows that there is no phase shift between v2 and i2 because the angle is $\theta = 0°$ so that means is it is working on resonance frequency on the inductive region switching (ZVS). The second scope displays the simulated instantaneous value for p2 at the secondary AC circuit. This will achieve the maximum output power at the minimum input VA rating at the receiver stage [14].

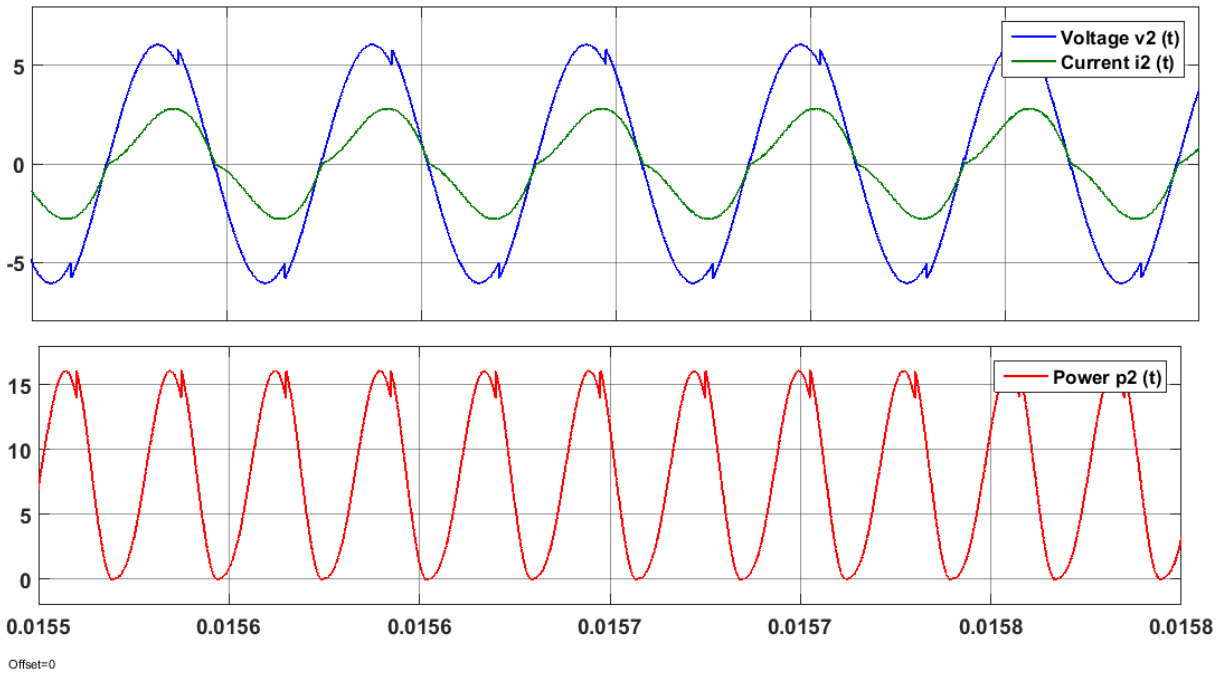

Fig 4.24 Simulated instantaneous values for v2, i2 and p2 at the secondary AC circuit

At the secondary DC circuit (Blue section)

Table 4.8 shows the experimented, simulated and calculated values of voltage, current and power at section 4 of Fig 3.2

Table 4.8 Comparison for the Mean values of Vload, Iload and Pload at secondary DC circuit

Parameters on 4th Section	**Experimented**	**Simulated**	**Calculated**
Vload Voltage Mean value	2.12 V	3.19 V	-
ILoad Current Mean value	1.33 A	1.64 A	-
Pload Power value	2.8 W	5.1 W	-
η Efficiency of the system = Pload/Pdc	10 %	16.9 %	-

The screen of the oscilloscope In Fig 4.25 display the experimental AC Input v2 in yellow color and the output DC Vload in blue color through the rectifier when there is no load (open circuit)

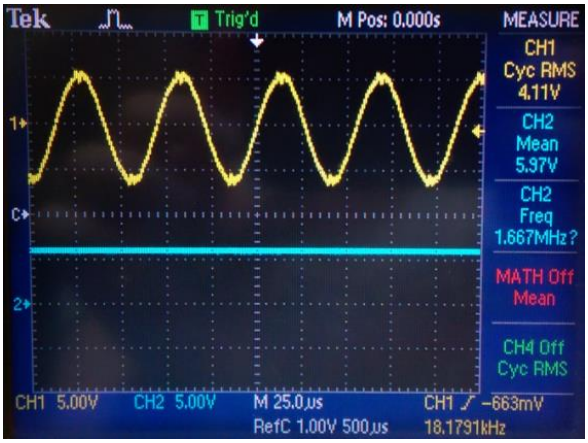

Fig 4.25 Experimental voltage input and output through the rectifier with no load

The first scope in Fig 4.26 display the simulated AC input voltage v2 and the second scope display the simulated DC output voltage vload through the full wave rectifier when there is no load (Open circuit)

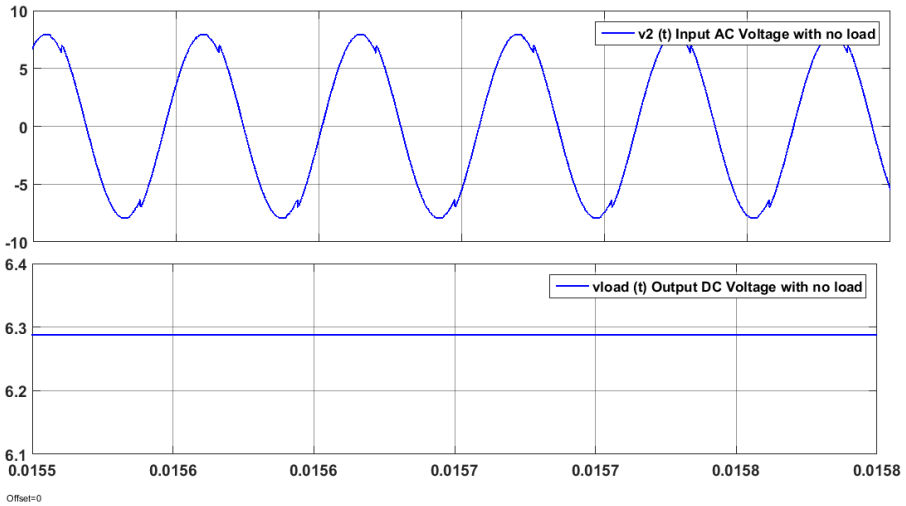

Fig 4.26 Simulated voltage input and output with no load through the rectifier

The screen of the oscilloscope in Fig 4.27 display the experimental AC input v2 in yellow color and the DC output vload in blue color through the full wave rectifier when there is 1.9Ω load. We can see the smoothing capacitor converts the full-wave rippled output of the rectifier into a smooth DC output voltage with some superimposed ripples.

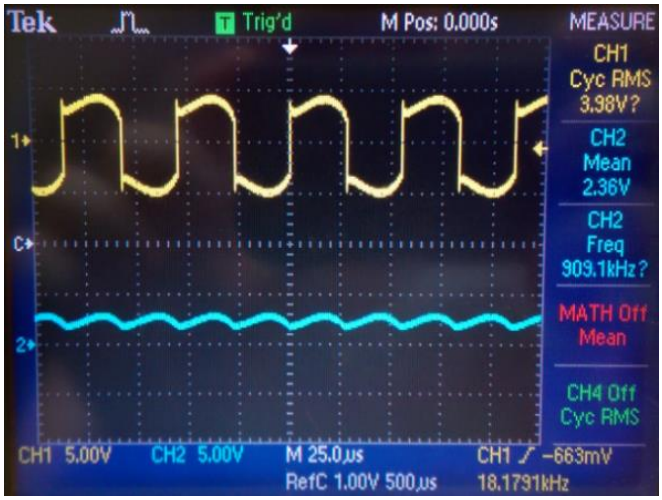

Fig 4.27 Experimental voltage input and output with load through the rectifier

The first scope in Fig 4.28 display the simulated AC input v2 and the second scope display the simulated DC output voltage vload through the full wave rectifier when there is 1.9Ω load.

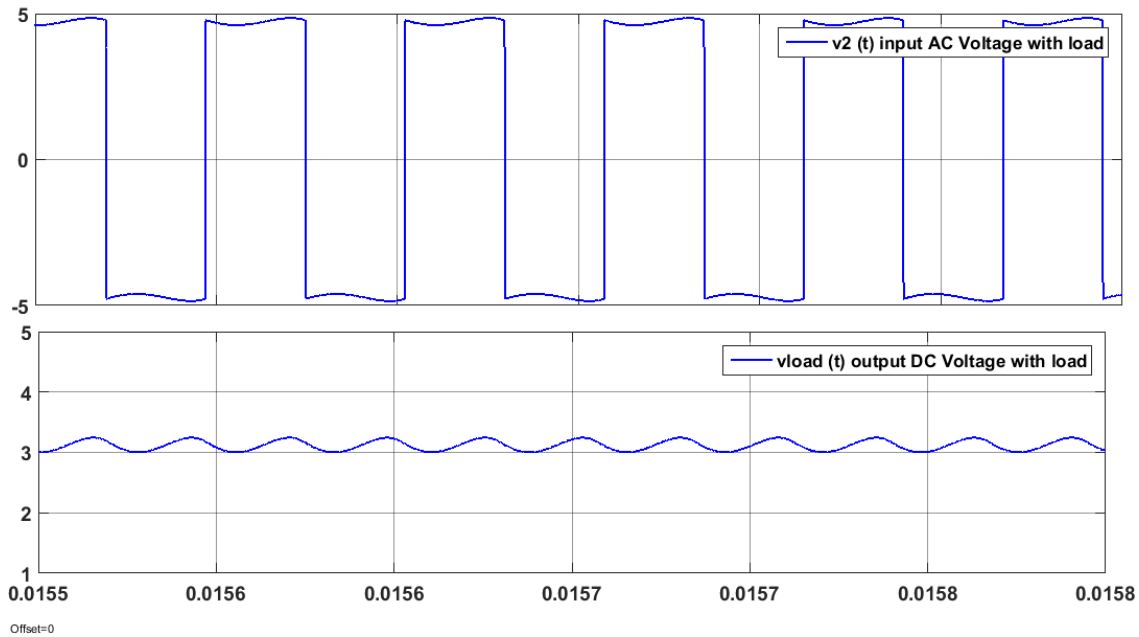

Fig 4.28 Simulated voltage input and output with load through the rectifier

The screen of the oscilloscope In Fig 4.29 display the experimental instantaneous DC vload in yellow, iload in blue and pload in red at the secondary DC circuit. It can be seen that the voltage vload have superimposed ripples and doesn't have perfect steady DC voltage, to improve this and smoother the voltage it is recommended to use bigger capacitor for the full wave bridge rectifier.

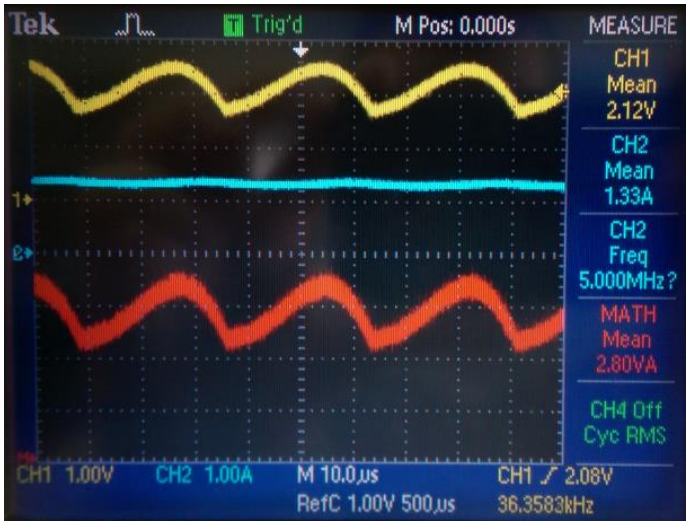

Fig 4.29 Experimental instantaneous values for vload, iload and pload at secondary DC circuit

The scopes in Fig 3.30 display the generated signals of the simulated instantaneous values for vload in blue color, iload in green color and pload in red color.

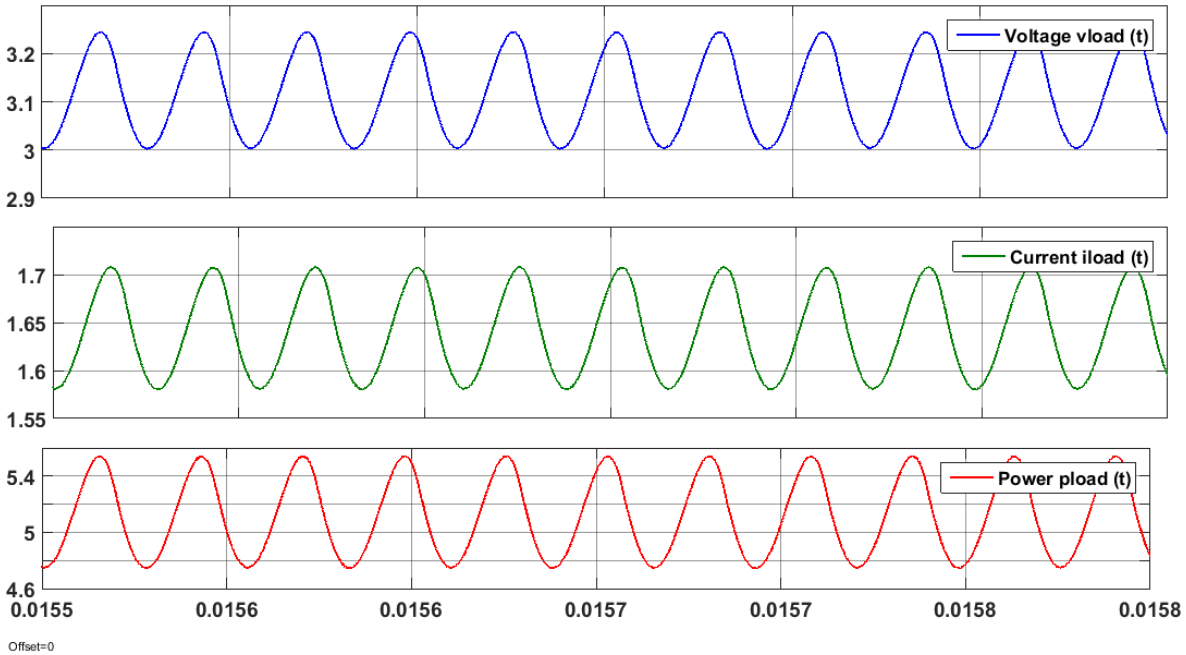

Fig 4.30 Simulated instantaneous values for vload, iload and pload at the secondary DC circuit

4.4.3 Intended Performance

At the beginning of this project, I had intended to achieve a peak overall efficiency of 58%. However, I quickly discovered that such efficiency was simply not possible to be achieved with the equipment of the lab due to the limitation of the power supply used, the unavailability of MOSFETs inverters and Litz-wire and even if there was a powerful power supply, some of the combined capacitors were used cannot handle high current.

All of the testing and research that I did on the experimental setup showed when supplying the inverters with 4 Volts the efficiency was 8% and when increased the power supply to the maximum possible 6 Volts at 5 Amps the efficiency increased to 10 % when the coils were separated by 3cm. However, using the same experimental setup and configuration would give a better efficiency if a powerful power supply and appropriate components were used at higher Voltage-Ampere levels.

CHAPTER 5

Conclusion and Future Work

5.1 Conclusion

The method used to calculate the self-inductance of rectangular coil with multiple numbers of turns was proven to be valid and the method to calculate the mutual inductance between two coils was found to be good. It was observed that the selection of an appropriate compensation topology is very important to start the design with. A good analysis for the system would lead to a better efficiency result within the electrical allowed specifications for voltage and current, for this purpose series-series topology was chosen and analyzed.

It was found that keeping the primary circuit at resonance would lead to the minimum VA requirements for the inverters. For a better coupling between the coils it was found by increasing the number of turns on each coil will lead to a better coupling between the coils. However the better coupling between the coils the less frequency required to transfer the power.

Through the testing of the project, it was found that wireless power transfer can result to a good level, but the efficiency still a big challenge and need more research to reach a better level. Resonant coupling seems to be the technology of the future for wireless power transfer.

5.2 Future Work

Further investigation about combining different compensations at once and adding a frequency controller for charging the battery.

References

[1] W.C. Brown, "The history of wireless power transmission," Solar Energy, vol.56, no.1, pp. 3-21, Jan. 1996

[2] Chao Liu Hu, A.P. Nair, N.K.C. Covic, G.A. "2-D alignment analysis of capacitively coupled contactless power transfer systems," Energy Conversion Congress and Exposition (ECCE), 2010 IEEE, vol, no, pp.652-657, 12-16 Sept. 2010

[3] http://witricity.com/applications/

[4] Wireless Power Transfer for Medical Microsystems: Tianjia Sun • Xiang Xie • Zhihua Wang Tsinghua University Beijing, ISBN: 978-1-4614-7701-3 (Print) 978-1-4614-7702-0 (Online)

[5] Resonant LLC Converter: Operation and Design Application Note AN2012-09 V1.0 Sep 2012

[6] Rui Chen, Cong Zheng, Zahid, Z.U, Faraci, Wengsong Yu, Jih-Sheng Lai, Senesky, M. Anderson, D, Lisi, G., "Analysis and parameters optimization of a contactless IPT system for EV charger," Applied Power Electronics Conference and Exposition (APEC), 2014 Twenty-Ninth Annual IEEE, pp.1654-1661, lb- 20 March 2014

[7] Comparative study of series-series and series parallel topology for long track EV charging application. Kunwar Aditya, Student Member, IEEE, and Sheldon S. Williamson, Senior Member, IEEE Conference Paper June 2014.

[8] Development of an inductively coupled power transfer system (ICPT) for electric vehicles with a large airgap. J.L.Villa, A. Llombart, J.F.Sanz , J.SallanElectric Engineering Department, University of Zaragoza C/María de Luna 3, 50018, Zaragoza, Spain.

[9] Inductively coupled power transfer (ICPT) for electric vehicle charging - A review. Kafeel Ahmed Kalwar, Muhammad Aamir, Saad Mekhilef. Renewable and Sustainable Energy Reviews 47 (2015) 462–475.

[10] O. Jonah and S. Georgakopoulos, “Wireless power transfer in concrete via strongly coupled magnetic resonance,” IEEE Transactions on Antennas and Propagation, vol. 61, no. 3, pp. 1378–1384, March 2013.

[11] Wireless Power Transfer: Survey and Roadmap Xiaolin Mou, Student Member, IEEE and Hongjian Sun, Member, IEEE. February 18, 2015

[12] Design Considerations of Compensation Topologies in ICPT System: Wenqi Zhou, Hao Ma College of Electrical Engineering, Zhejiang University, Hangzhou, China

[13] Parameters design method of magnetic coupled coil in ICPT system: Jianghua Lu1*, Junkun Zhang1, Wenjing Li1 Guo-Rong Zhu1, 2 and Tingting Wang21 School of Automation, Wuhan University of Technology, Wuhan, China

[14] Series-series resonant IPT system analysis under frequency mismatch: Manuele Bertoluzzo,* Rupesh Kr. Jha,**Student Member, IEEE, and Giuseppe Buja,*** Life Fellow IEEE Department of Industrial Engineering, University of Padova, Padova, Italy.

Appendix A

Program 1 Matlab codes

1.1 Matlab Code 1 Parameters Calculations

```
f=18000; % frequency Hz
u0=4*pi*1e-7; % phi permeability of the air
w0=2*pi*f; % resonance frequency
L=0.45; % m Length of the primary coil
d=0.25;% m width of the coils
h=0.03; % m Height
a=0.1; % m length of the primary coil
N1=12; % number of turns for coil 1
N2=12; % number of turns for coil 2
S1=10e-6; % mm2 sections of the windings 1 USE IT FOR CALCULATE L1 C1
S2=30e-6; % mm2 sections of the windings 2 USE IT FOR CALCULATE L2 C2
%S1=1; % Used To CALCULATE (RES1)
%S2=3; % Used To CALCULATE (RES1)

% Find the equivalent radius of the windings
R1=sqrt(N1*S1/pi);
R2=sqrt(N2*S2/pi);

% Find L1 L2
L1=u0/pi*N1^2*d*log(2*L*d/(R1*(d+sqrt(L^2+d^2))))+u0/pi*N1^2*(L*log(2*L*d/(R1
*(L+sqrt(L^2+d^2))))-2*(d+L-sqrt(d^2+L^2)))+u0*N1^2*(L+d)/(4*pi);
L2=u0/pi*N2^2*d*log(2*a*d/(R2*(d+sqrt(a^2+d^2))))+u0/pi*N2^2*(a*log(2*a*d/(R2
*(a+sqrt(a^2+d^2))))-2*(d+a-sqrt(d^2+a^2)))+u0*N2^2*(a+d)/(4*pi);

% Mutual inductance when the two coils have the same dimensions
M=((((u0/pi)*(N1*N2))*(d*log((d+(sqrt(h^2+d^2))*sqrt((h^2)+(a^2)))/(d+h*sqrt(
(h^2)+(d^2)+(a^2))))))+(((u0/pi)*(N1*N2))*(a*log((a+sqrt((h^2)+(d^2))*sqrt((h
^2)+(a^2)))/(a+h*sqrt((h^2)+(d^2)+(a^2))))))+(((u0/pi)*(N1*N2))*(2*(h-
sqrt((h^2)+(d^2))-sqrt((h^2)+(a^2))+sqrt((h^2)+(d^2)+(a^2))))));

% Mutual inductance considering a case where the primary track is longer than
the secondary pick up, L >> a
M1=((u0/pi)*N1*N2*a*log(sqrt((h^2)+(d^2))/h));

% Find Resistance of the coils Res1 and Res2
Res1=((1/57)*N1*((2*(L+d))/S1)); % resistive value of the windings
Res2=((1/57)*N2*((2*(a+d))/S2)); % resistive value of the windings

% Find C1 and C2
C1=1/((2*pi*f)^2*L1); % Capacitor 1
C2=1/((2*pi*f)^2*L2); % Capacitor 2

% Find coupling coefficient K
K=(M1/(sqrt(L1*L2)));

% Second way to calculate the resonance frequency
wo=(1/sqrt(L1*C1));
```

1.2 Matlab Code 2 Parameters Calculations

```
f=18000;
w0=2*pi*f;
N1=12;
N2=12;
L1=1.384728220516740e-04;
L2=4.198743060041229e-05;
C1=5.645867867181731e-07;
C2=1.861984039794621e-06;
Res1=0.294736842105263;
Res2=0.049122807017544;
M1=1.225389420605090e-05;

V1=17; % Input Voltage
VLoad=20; % Input Desired output voltage
ILoad=6; % Input Desired output current

% Find RLoad the terminal load resistance
RLoad=VLoad/ILoad;

% Find the Equivalent load resistance RL
n=N1/N2;
RL=((8*n^2)/(pi^2))*RLoad;

% Find the Equivalent impedance for secondary side
Z2=Res2+(1/(1i*w0*C2))+(1i*w0*L2)+RL;

% Find the Equivalent impedance for all circuit
Ztotal=(Res1+(1i*w0*L1)+(1/(1i*w0*C1))+(((w0^2)*(M1^2))/Z2));

%Find I1 the current through the primary side when at resonance
I1=V1/Ztotal;
I11=V1/(Res1+(w0^2*M1^2/(Res2+RL))); % used when at resonance

%Find I2 the current through the second side
I2=I1*(1i*w0*M1)/Z2;

% Find V2 the voltage Induced in secondary coil
V2=(1i*w0*M1)*(I1-I2);

% Find The power at the primary side P1
P1=V1^2/(Res1+((w0^2*M1^2)/(Res2+RL))); % used when at resonance

% Find The power transferred from the primary to the secondary P2
P2=(I1^2)*((w0^2*M1^2)/RLoad);

% Find the EFFICIENCY
efficiency=P2/P1;
```

Appendix B

Program 2 Matlab codes

2.1 Matlab Code 1 Parameters Calculations

```
f=18182; % Switching Frequency
L1=94.66e-6; % inductance of the primary coil measured from LCR meter
L2=21.73e-6; % inductance of the secondary coil measured from LCR meter

% Find C1 and C2
C1=1/((2*pi*f)^2*L1); % Capacitor 1
C2=1/((2*pi*f)^2*L2); % Capacitor 2
```

2.2 Matlab Code 2 Parameters Calculations

```
f=18182; % Switching Frequency
w0=2*pi*f;
N1=12;
N2=12;
L1=94.66e-6; % inductance of the primary coil
L2=21.73e-6; % inductance of the secondary coil
Res1=0.55; % Resistance of the primary coil + wires
Res2=0.047; % Resistance of the secondary coil + wires
C1=783e-9; % real experimental value for the set of the capacitors combined
C2=3700e-9; % real experimental value for the set of the capacitors combined
M1=6.12e-6; % mutual inductance at 3 cm height between L1 and L2
V1=6; % Input Voltage
RLoad=1.9; % INPUT terminal load resistance RLoad

% Find the Equivalent load resistance RL
n=N1/N2;
RL=((8*n^2)/(pi^2))*RLoad;

% Find the Equivalent impedance for secondary side
Z2=Res2+(1i*((w0*L2)-(1/(w0*C2))))+RL;

% Find the Equivalent impedance for all circuit used when out of resonance
Ztotal=(Res1+(1i*w0*L1)+(1/(1i*w0*C1))+(((w0^2)*(M1^2))/Z2));

%Find I1 the current through the primary side
I1=V1/Ztotal;

%Find I2 the current through the second side
I2=I1*(1i*w0*M1)/Z2;

% Find V2 the voltage Induced in secondary coil
V2=(1i*w0*M1)*(I1-I2);

% Find The power at the primary side P1
P1=(V1^2*(Res2+RL))/((Res1*Res2)+(Res1*RL)+(w0^2*M1^2))^2;

% Find The power transferred from the primary to the secondary P2
P2=(I1^2*w0^2*M1^2)/RLoad;

% Find the EFFICIENCY
efficiency=P2/P1;
```